R. G. Kouyoumjian

The Geometrical Theory of Diffraction and Its Application

R. G. Kouyoumjian

The Geometrical Theory of Diffraction and Its Application

6. The Geometrical Theory of Diffraction and Its Application

R. G. KOUYOUMJIAN

With 15 Figures

The rigorous treatment of the diffraction from radiating systems (scatterers and antennas) using the eigenfunction method or the method of Rayleigh, which is based upon the expansion of the field in inverse powers of wavelength, is limited to those objects whose surfaces coincide with the surfaces of orthogonal curvilinear coordinates. Moreover, the solutions obtained are poorly convergent for objects more than a wavelength or so in extent.

Recently there has been considerable interest in the integral-equation formulation of the radiation problem, and its solution by the moment method. Arbitrary shapes can be handled by this method, but in general numerical results also are restricted to objects not large in terms of a wavelength, because of the limitations of present-day computers.

When a radiating object is large in terms of a wavelength the scattering and diffraction is found to be essentially a local phenomenon identifiable with specific parts of the object, e.g., points of specular reflection, shadow boundaries, and edges. The high-frequency approach to be discussed in this chapter employs rays in a systematic way to describe this phenomenon. It was originally developed by KELLER and his associates at the Courant Institute of Mathematical Sciences. This method referred to as the geometrical theory of diffraction is approximate in nature, but in many examples it appears to yield the leading terms in the asymptotic high-frequency solution. Moreover, in many cases it works surprisingly well on radiating objects as small as a wavelength or so in extent. Thus if a solution is desired over a wide spectral range, this high-frequency method nicely complements the low-frequency methods described in the second and third chapters. Finally it will be seen to be sufficiently flexible so that it can be combined with the moment method thereby extending the class of solutions for either method used separately.

The treatment of high-frequency diffraction to follow is restricted to perfectly conducting objects located in isotropic, homogeneous media. The method presented, however, can be extended to penetrable objects and to inhomogeneous and anisotropic media.

6.1. Asymptotic Solution of Maxwell's Equations

6.1.1. Geometrical Optics

Let us begin by examining an asymptotic high-frequency solution to Maxwell's equations in a source-free region occupied by an isotropic, homogeneous medium. Our approach follows that introduced by LUNEBERG [6.1] and KLINE [6.2, 3]. From Maxwell's equations the electric field is found to satisfy

$$\nabla^2 E + k^2 E = 0 \tag{6.1}$$

subject to the condition that

$$\nabla \cdot E = 0 . \tag{6.2}$$

The phase constant $k = \omega\sqrt{\varepsilon\mu}$, where ω is the angular frequency, ε is the permittivity of the medium, and μ is the permeability; a time dependence of $\exp(j\omega t)$ is assumed.

The Luneberg-Kline expansion of the electric field for large ω is

$$E(R, \omega) = \mathrm{e}^{-jk_0\psi(R)} \sum_{m=0}^{\infty} \frac{E_m(R)}{(j\omega)^m} \tag{6.3}$$

in which R is the position vector, and k_0 is the phase constant of empty space. Substituting (6.3) into (6.1) and (6.2) and equating like powers of ω, one obtains the eikonal equation

$$|\nabla\psi|^2 = n^2 \tag{6.4}$$

together with the first-order transport and conditional equations

$$\frac{\partial E_0}{\partial s} + \frac{1}{2}\left(\frac{\nabla^2 \psi}{n}\right) E_0 = 0 , \tag{6.5}$$

$$\hat{s} \cdot E_0 = 0 , \tag{6.6}$$

plus higher-order transport and conditional equations which do not concern us here. In the preceding equations $\hat{s} = \nabla\psi/n$ is a unit vector in the direction of the ray path, and s is the distance along the ray path.

We are interested here in the solution at the high-frequency limit, so the asymptotic approximation for E reduces to

$$E(s) \sim \mathrm{e}^{-jk_0\psi(s)} E_0(s) . \tag{6.7}$$

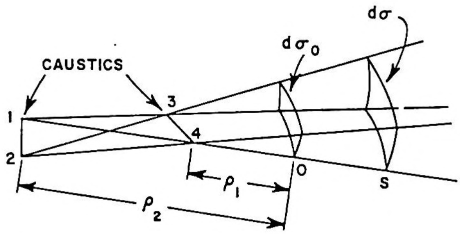

Fig. 6.1. Astigmatic tube of rays

Equation (6.5) is readily integrated and after some manipulation one obtains [6.4, 5].

$$E(s) \sim E_0(0)\, e^{-jk_0\psi(0)} \sqrt{\frac{\varrho_1 \varrho_2}{(\varrho_1+s)(\varrho_2+s)}}\, e^{-jks} \tag{6.8}$$

in which $s=0$ is taken as a reference point on the ray path, and ϱ_1, ϱ_2 are the principal radii of curvature of the wavefront at $s=0$. In Fig. 6.1 ϱ_1 and ϱ_2 are shown in relationship to the rays and wavefronts.

Equation (6.8) is commonly referred to as the geometrical-optics field, because it could have been determined in part from classical geometrical optics. Specifically the quantity under the square root, the divergence factor, follows from conservation of power in a tube of rays; in addition, we note that the eikonal equation could have been deduced from Fermat's principle, a fundamental postulate of classical geometrical optics. As is well known, classical geometrical optics ignores the polarization and wave nature of the electromagnetic field; however, the leading term in the Luneberg-Kline asymptotic expansion is seen to contain this missing information.

It is apparent that when $s=-\varrho_1$ or $-\varrho_2$, $E(s)$ given by (6.8) becomes infinite, so that this asymptotic approximation is no longer valid. The intersection of the rays at Lines 1–2 and 3–4 of the astigmatic tube of rays is called a caustic. As we pass through a caustic in the direction of propagation, $\varrho+s$ changes sign and the correct phase shift of $+\pi/2$ is introduced naturally. Equation (6.8) is a valid high frequency approximation on either side of the caustic; however the field at the caustic must be found from separate considerations [6.6, 7].

Employing the Maxwell curl equation $\nabla X E = -j\omega\mu H$, it follows from (6.3) that the leading term in the asymptotic approximation for the magnetic field is

$$H \sim \hat{s} \times E/Z_c\,, \tag{6.9}$$

where $Z_c = \sqrt{\mu/\varepsilon}$ is the characteristic impedance of the medium, and E is given by (6.8).

6.1.2. Reflection

Geometrical optics provides a high-frequency approximation for the incident, reflected and refracted fields. Let us find the geometrical optics field

$$E^{rg}(s) = e^{-jk_0\psi^r(s)} E_0^r(s) \tag{6.10}$$

reflected from the point Q_R on a perfectly-conducting smooth curved surface S; the distance between Q_R and the field point on the reflected ray is denoted by s. The outward directed unit normal vector at Q_R is $\hat{n}$, and $\hat{s}^i$ and $\hat{s}^r$ are unit vectors in the directions of incidence and reflection, respectively, as shown in Fig. 6.2.

From the boundary condition on the total electric field at Q_R on S,

$$\hat{n} \times (E^i + E^r) = 0\,, \tag{6.11}$$

it can be shown that

$$E_0^r(Q_R) = E_0^i(Q_R) \cdot \underset{\sim}{R} = E_0^i(Q_R) \cdot [\hat{e}_{\parallel}^i \hat{e}_{\parallel}^r - \hat{e}_{\perp}\hat{e}_{\perp}] \tag{6.12}$$

where $\hat{e}_{\perp}$ is a unit vector perpendicular to the plane of incidence, and $\hat{e}_{\parallel}^i$, $\hat{e}_{\parallel}^r$ are unit vectors parallel to the plane of incidence so that

$$\hat{e}_{\parallel} = \hat{e}_{\perp} \times \hat{s}\,. \tag{6.13}$$

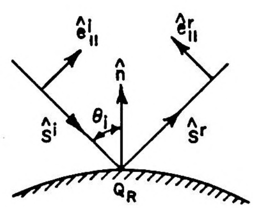

Fig. 6.2. Reflection at a curved surface

In matrix notation the reflection coefficient has a form familiar for the reflection of a plane electromagnetic wave from a plane, perfectly-conducting surface, namely

$$R = \begin{bmatrix} 1 & 0 \\ 0 & -1 \end{bmatrix}. \tag{6.14}$$

This is not surprising if one considers the local nature of high-frequency reflection, i.e., the phenomenon for the most part depends on the geometry of the problem in the immediate neighborhood of Q_R. Note that the incident and reflected fields must be phase matched on S to satisfy (6.11), i.e.,

$$\psi^i(Q_R) = \psi^r(Q_R). \tag{6.15}$$

The above equality leads to the law of reflection, and it is also employed to obtain (6.12).

The geometrical optics reflected field is

$$E^{rg}(s) = E^{ig}(Q_R) \cdot \underset{\sim}{R} \sqrt{\frac{\varrho_1^r \varrho_2^r}{(\varrho_1^r + s)(\varrho_2^r + s)}}\, e^{-jks} \tag{6.16}$$

in which ϱ_1^r, ϱ_2^r are the principal radii of curvature of the reflected wavefront at Q_R. It can be shown that

$$\frac{1}{\varrho_1^r} = \frac{1}{2}\left(\frac{1}{\varrho_1^i} + \frac{1}{\varrho_2^i}\right) + \frac{1}{f_1} \tag{6.17}$$

$$\frac{1}{\varrho_2^r} = \frac{1}{2}\left(\frac{1}{\varrho_1^i} + \frac{1}{\varrho_2^i}\right) + \frac{1}{f_2}. \tag{6.18}$$

The above equations are reminiscent of the simple lens and mirror formulas of elementary physics; this is particularly true of an incident spherical wave, where $\varrho_1^i = \varrho_2^i = s'$. Expressions for f_1 and f_2 are given in [6.8]. For an incident spherical wave,

$$\begin{aligned} \frac{1}{f_{\frac{1}{2}}} = {} & \frac{1}{\cos\theta_i}\left(\frac{\sin^2\theta_2}{a_1} + \frac{\sin^2\theta_1}{a_2}\right) \\ & \pm \sqrt{\frac{1}{\cos^2\theta_i}\left(\frac{\sin^2\theta_2}{a_1} + \frac{\sin^2\theta_1}{a_2}\right)^2 - \frac{4}{a_1 a_2}} \end{aligned} \tag{6.19}$$

in which θ_1 and θ_2 are the angles between $\hat{s}^i$ and the principal directions associated with the principal radii of curvature of the surface a_1 and a_2, respectively. In the case of plane wave illumination it follows from (6.17–19),

$$\sqrt{\varrho_1^r \varrho_2^r} = \sqrt{a_1 a_2}/2 \tag{6.20}$$

which is useful in calculating the far-zone reflected field.

If a_1 or a_2 become infinite, as in the case of a flat plate or cylindrical scatterers, it is evident that geometrical optics fails. Geometrical optics approximates the scattered field only in the direction of specular reflection, as determined by the law of reflection.

In principle the geometrical-optics approximation can be improved by finding the higher-order terms E_1, $E_2, \ldots$ in the Luneberg-Kline expansion. Luneberg-Kline expansions for fields reflected from cylinders, spheres and other curved surfaces with simple geometries are given in [6.9]. These terms improve the high-frequency approximation of the scattered field if the specular point is well away from shadow boundaries, edges or other surface discontinuities; however, it is noted that they tend to become singular as the specular point approaches close to a shadow boundary on the surface. Furthermore, these terms do not describe the diffracted field which penetrates into the shadow region, nor do they correct the discontinuities in the geometrical-optics field at shadow and reflection boundaries. An examination of available asymptotic solutions for diffracted fields reveals that they contain fractional powers of ω. Furthermore, one notes that caustics of the diffracted field are located at the boundary surface. From these considerations it is evident that the Luneberg-Kline series cannot be used to treat diffraction. At the present time additional postulates are required to introduce the high-frequency diffracted field; these are given in the next subsection.

It should ne noted, however, that for ω sufficiently large the geometrical-optics field may require no correction, i.e., the scattering phenomenon is entirely dominated by geometrical optics. This is the case for backscatter from smooth curved surfaces with radii of curvature very large in terms of a wavelength.

6.1.3. Diffraction

To overcome the limitations of the geometrical-optics field pointed out at the end of the last subsection, it is necessary to introduce an additional field, the diffracted field. KELLER [6.10–12] has shown how the diffracted field may be included in the high-frequency solution as an extension of geometrical optics. The postulates of Keller's theory, commonly referred to as the geometrical theory of diffraction (GTD), are summarized as follows.

(1) The diffracted field propagates along rays which are determined by a *generalization of Fermat's principle* to include points on the boundary surface in the ray trajectory.

2) Diffraction like reflection and transmission is a *local phenomenon* at high frequencies, i.e., it depends only on the nature of the boundary surface and the incident field in the immediate neighborhood of the point of diffraction.

3) The diffracted wave propagates along its ray so that

a) power is conserved in a tube (or strip of rays),

b) the phase delay along the ray path equals the product of the wave number of the medium and the distance.

The diffracted rays which pass through a given field point are found from the generalized Fermat's principle. The notion that points on the boundary surface may be included in the ray trajectory is not new. Imposing the condition that a point on a smooth curved surface be included in the ray path between the source and observation point is a time-honored method for deducing the reflected ray and the law of reflection. It seems reasonable to extend the class of such points as KELLER has done. Diffracted rays are initiated at points on the boundary surface where the incident geometrical-optics field is discontinuous[1], i.e., at points on the surface where there is a shadow or reflection boundary of the incident field. Examples of such points are edges, vertices and points at which the incident ray is tangent to a smooth, curved surface. The diffracted rays like the geometrical-optics rays follow paths which make the optical distance between the source point and the field point an extremum, usually a minimum. Thus the portion of the ray path which traverses a homogeneous medium is a straight line, and if a segment of the ray path lies on a smooth surface, it is a surface extremum or geodesic.

For points away from the diffracting surface, Postulate 3 of Keller's theory actually follows from his first two postulates. Consider a normal congruence of rays emanating from a point of diffraction on the radiating surface. The high-frequency diffracted field at P, see Fig. 6.3, may be found by asymptotically approximating its integral representation

$$E^{d}(s) = \int F \, e^{-jkr} \, da \,. \tag{6.21}$$

[1] The incident field may be a diffracted field; a discontinuity of the diffracted field on the boundary surface initiates a higher-order diffracted ray.

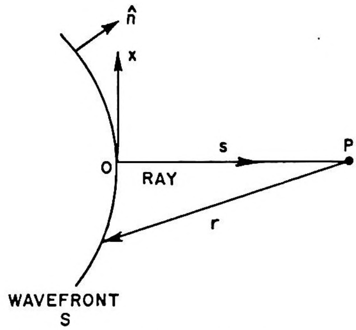

Fig. 6.3. Ray and wavefront geometry

The integral is taken over a wavefront associated with the diffracted rays and

$$F = \frac{jkZ_c}{4\pi r}\left\{\hat{r}\times[\hat{r}\times(\hat{n}\times H^d)] - \frac{1}{Z_c}\hat{r}\times(E^d\times\hat{n})\right\} \tag{6.22}$$

in which $\hat{n}$ is the unit normal vector to the wavefront and the other quantities are defined in Fig. 6.3. Then employing (6.9) together with the approximations

$$r \approx s + \frac{x^2}{2}\left(\frac{1}{s}+\frac{1}{\varrho_1}\right) + \frac{y^2}{2}\left(\frac{1}{s}+\frac{1}{\varrho_2}\right)$$

and

$$da \approx dx\,dy/\hat{n}\cdot\hat{s}$$

in which x, y are rectangular coordinates perpendicular to s at 0, one obtains

$$E^d(s) \sim E^d(0)\sqrt{\frac{\varrho_1\varrho_2}{(\varrho_1+s)(\varrho_2+s)}}\,e^{-jks} \tag{6.23}$$

by using the method of stationary phase [6.13, 14]. Equation (6.23) has the same form as (6.8), which is not an unexpected result, because this development also can be applied to the incident and reflected fields of geometrical optics; however, it does not yield higher-order terms as does the Luneberg-Kline expansion.

In calculating the diffracted field it is convenient to choose the point of diffraction on the boundary surface as the reference point 0. However, this point of diffraction is also a caustic of the diffracted ray. First consider the case where the caustic is at an edge or forms a line on a smooth convex surface from which rays shed tangentially. Either ϱ_1 or ϱ_2 denoted by ϱ' vanishes; however, $E^d(s)$ must be independent of the location of the reference point; hence it follows from (6.23) that

$$\lim_{\varrho' \to 0} E^d(0)\sqrt{\varrho'} = C \tag{6.24}$$

exists, so that

$$E^d(s) = C\sqrt{\frac{\varrho}{s(\varrho+s)}}\, e^{-jks} \tag{6.25}$$

in which ϱ is the distance between the caustic on the boundary surface (the point of diffraction) and the second caustic of the diffracted ray, which is away from this surface. Thus the diffracted rays, like the geometrical-optics rays form an astigmatic tube, as shown in Fig. 6.1 with either the caustic 1–2 or 3–4 at the point of diffraction on the boundary surface. The caustic distance ϱ may be determined by differential geometry; an expression for ϱ will be given later.

For a two-dimensional problem we note that $\varrho = \infty$, so (6.25) reduces to

$$E^d(s) = C\,\frac{e^{-jks}}{\sqrt{s}}. \tag{6.26}$$

Next let us consider the diffraction from a vertex or corner, where the diffracted rays emanate from a point caustic at the tip. In this case $\varrho_1 = \varrho_2 = \varrho'$, and again since $E^d(s)$ must be independent of the reference point $s = 0$, it follows from (6.23) that

$$\lim_{\varrho' \to 0} E^d(0)\,\varrho' = B \tag{6.27}$$

exists, and so for vertex or corner diffraction

$$E^d(s) = B\,\frac{e^{-jks}}{s}. \tag{6.28}$$

Diffraction is a local effect according to Postulate 2, and since we are dealing with a linear phenomenon, C and B must be proportional to the incident field at the point of diffraction, if the incident field is not rapidly varying there[2]. The constant of proportionality is referred to as a diffraction coefficient, and for electromagnetic fields it is a dyadic. It is convenient to determine this from the asymptotic solution of the simplest boundary value problem having the same local geometry as that near the point of diffraction. A problem of this type is referred to as a canonical problem; canonical problems are employed to determine the diffraction coefficients for edges, the diffraction coefficients and attenuation constants for smooth curved surfaces, and other parameters of the GTD.

6.2. Edge Diffraction

6.2.1. The Wedge

Let us consider the field radiated from a point source at 0 and observed at P in the presence of a perfectly-conducting wedge, as shown in Fig. 6.4a, where the rays are projected on a plane perpendicular to the edge at the point of diffraction Q_E. Applying the generalized Fermat's principle, the distance along the ray path $0Q_EP$ is a minimum and the law of edge diffraction

$$\hat{s}' \cdot \hat{e} = \hat{s} \cdot \hat{e} \tag{6.29}$$

results. Here $\hat{e}$ is a unit vector directed along the edge, and $\hat{s}'$ and $\hat{s}$ are unit vectors in the directions of incidence and diffraction, respectively. The above equation also follows from the requirement that the incident and diffracted fields be phase matched along the edge. If the incident ray strikes the edge obliquely, making an angle β_0' with the edge, as shown in Fig. 6.4b, the diffracted rays lie on the surface of a cone whose half angle is equal to β_0'. The position of the diffracted ray on this conical surface is given by the angle ϕ, and the direction of the ray incident on the edge, by the angles ϕ' and β_0'; these angles are defined in Fig. 6.4a and b. Equation (6.29) may be used to develop a computer search program to locate the points of edge diffraction.

From (6.25) and the discussion following, the expression for the electric field of the edge-diffracted ray is

$$E^d(s) = E^i(Q_E) \cdot \underset{\sim}{D}(\phi, \phi'; \beta_0') \sqrt{\frac{\varrho}{s(\varrho + s)}}\, e^{-jks} \tag{6.30}$$

[2] If the incident field is rapidly varying at the point of diffraction, it may be possible to separate it into slowly-varying components for the purpose of calculating the diffracted field.

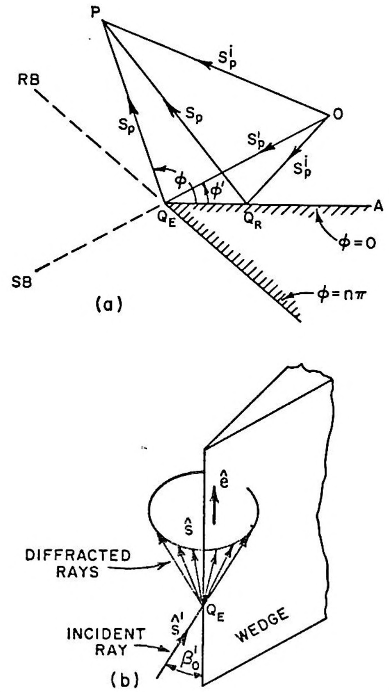

Fig. 6.4a and b. Reflection and diffraction from a wedge. The subscript p indicates that the ray path is shown projected on a plane perpendicular to the edge

in which $\underset{\sim}{D}(\phi, \phi'; \beta_0')$ is the dyadic edge-diffraction coefficient. Since the pertinent dimension in wedge diffraction is wavelength, it follows from dimensional considerations that the diffraction coefficient must vary as $k^{-1/2}$. The dyadic diffraction coefficient for a perfectly-conducting wedge has been obtained by KOUYOUMJIAN and PATHAK; their work is described in [6.8, 15] and will only be summarized here. As noted before, the dyadic diffraction coefficient can be found from the asymptotic solution of canonical problems, which in this case involve the illumination of the wedge by plane, cylindrical, conical and spherical waves. The solution of these canonical problems serves as a basis for deducing the dyadic diffraction coefficient for arbitrary wavefront illumination and for the more general case where there are curved edges and curved surfaces.

Let us introduce an edge-fixed plane of incidence containing the incident ray and the edge and a plane of diffraction containing the diffracted ray and the edge. The unit vectors $\hat{\phi}'$ and $\hat{\phi}$ are perpendicular to the edge-fixed plane of incidence and the plane of diffraction, respectively. The unit vectors $\hat{\beta}_0'$ and $\hat{\beta}_0$ are parallel to the edge-fixed plane of incidence and the plane of diffraction, respectively, and

$$\hat{\beta}_0' = \hat{s}' \times \hat{\phi}', \quad \hat{\beta}_0 = \hat{s} \times \hat{\phi}.$$

Thus the coordinates of the diffracted ray (s, β_0, ϕ) are spherical coordinates and so are the coordinates of the incident ray (s', β_0', ϕ'),

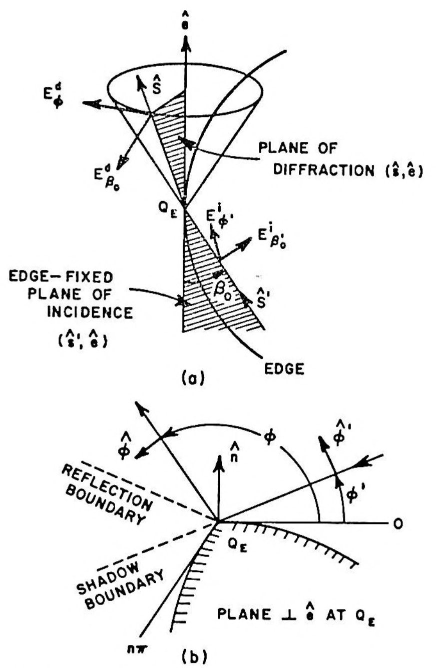

Fig. 6.5a and b. Diffraction by a curved edge

except that the incident (radial) unit vector points toward the origin Q_E. These ray-fixed coordinates and their unit vectors are shown in Figs. 6.4 and 6.5. Although the latter figure depicts curved edges and curved surfaces, it is still helpful in the present discussion (one may regard the wedge as just a special case of the curved edge structure).

For each type of edge illumination mentioned previously, it is shown in [6.15] that the dyadic diffraction coefficient can be represented simply as the sum of two dyads, if the ray-fixed coordinates mentioned in the preceding paragraph are used.

$$\underset{\sim}{D}(\phi, \phi'; \beta_0') = -\hat{\beta}_0' \hat{\beta}_0 \, D_s(\phi, \phi'; \beta_0') - \hat{\phi}' \hat{\phi} \, D_h(\phi, \phi'; \beta_0'), \tag{6.31}$$

where D_s is the scalar diffraction coefficient for the acoustically soft (Dirichlet) boundary condition at the surface of the wedge, and D_h is the scalar diffraction coefficient for the acoustically hard (Neumann) boundary condition. This result shows the close connection between electromagnetics and acoustics at high frequencies. If the dyadic diffraction coefficient is expressed in an edge-fixed coordinate system, it is found to be the sum of seven dyads. In matrix notation this means that the diffraction coefficient is a 3×3 matrix with seven non-vanishing elements, instead of the 2×2 diagonal matrix which may be used to represent the diffraction coefficient in the ray-fixed coordinate system. In this sense the ray-fixed coordinate system is the natural coordinate system of the problem.

If the field point is not close to a shadow or reflection boundary and $\phi' \neq 0$ or $n\pi$, the scalar diffraction coefficients

$$D_{\substack{s\\h}}(\phi, \phi'; \beta_0') = \frac{e^{-\frac{\pi}{4}} \sin \frac{\pi}{n}}{n\sqrt{2\pi k} \sin \beta_0'} \cdot \left[\frac{1}{\cos \frac{\pi}{n} - \cos\left(\frac{\phi - \phi'}{n}\right)} \mp \frac{1}{\cos \frac{\pi}{n} - \cos\left(\frac{\phi + \phi'}{n}\right)} \right] \tag{6.32}$$

for all four types of illumination, which is important because the diffraction coefficient should be independent of the edge illumination away from shadow and reflection boundaries. The wedge angle is $(2-n)\pi$, where the plane surfaces forming the wedge are $\phi = 0$ and $\phi = n\pi$, see Fig. 6.4a. This expression becomes singular as a shadow boundary (SB) or a reflection boundary (RB) is approached, which further aggravates the difficulties at these boundaries resulting from the discontinuities in the incident or reflected fields. The above scalar diffraction coefficients also have been given by KELLER [6.12]. The case of grazing incidence $\phi'=0$ or $n\pi$ will be considered later.

Expressions for the scalar diffraction coefficients which are valid at all points away from the edge (again excluding $\phi'=0$ or $n\pi$) are

$$D_{\substack{s\\h}}(\phi,\phi';\beta_0')=\frac{-e^{-j\frac{\pi}{4}}}{2n\sqrt{2\pi k}\sin\beta_0'}$$

$$\times\left[\cot\left(\frac{\pi+(\phi-\phi')}{2n}\right)F[kLa^{+}(\phi-\phi')]\right.$$

$$+\cot\left(\frac{\pi-(\phi-\phi')}{2n}\right)F[kLa^{-}(\phi-\phi')] \tag{6.33}$$

$$\mp\left\{\cot\left(\frac{\pi+(\phi+\phi')}{2n}\right)F[kLa^{+}(\phi+\phi')]\right.$$

$$\left.\left.+\cot\left(\frac{\pi-(\phi+\phi')}{2n}\right)F[kLa^{-}(\phi+\phi')]\right\}\right],$$

where

$$F(X)=2j|\sqrt{X}|\,e^{jX}\int_{|\sqrt{X}|}^{\infty}e^{-j\tau^2}d\tau\,. \tag{6.34}$$

When X is small

$$F(X)\simeq\left[\sqrt{\pi X}-2Xe^{j\frac{\pi}{4}}-\tfrac{2}{3}X^2e^{-j\frac{\pi}{4}}\right]e^{j\left(\frac{\pi}{4}+X\right)}, \tag{6.35}$$

and when X is large

$$F(X)\sim\left(1+j\frac{1}{2X}-\frac{3}{4}\frac{1}{X^2}-j\frac{15}{8}\frac{1}{X^3}+\frac{75}{16}\frac{1}{X^4}\right). \tag{6.36}$$

If the arguments of the four transition functions in (6.33) exeed 10, the transition functions are approximately equal to one, and (6.33) reduces to (6.32).

The argument of the transition function $X=kLa^{\pm}(\phi\pm\phi')$ in which L is a distance parameter which will be given later. The large parameter in the asymptotic approximation is kL. Let $\phi\pm\phi'=\beta$, then

$$a^{\pm}(\beta)=2\cos^2\left(\frac{2n\pi N^{\pm}-\beta}{2}\right) \tag{6.37}$$

in which $N^{\pm}$ are the integers which most nearly satisfy the equations

$$2\pi n N^{+} - \beta = \pi, \tag{6.38}$$

$$2\pi n N^{-} - \beta = -\pi. \tag{6.39}$$

Note that N^{+} and N^{-} each have two values.

$a^{\pm}(\beta)$ is a measure of the angular separation between the field point and a shadow or reflection boundary. The + and − superscripts are associated with the integers N^{+} and N^{-}, respectively, which are defined by (6.38) and (6.39). For exterior edge diffraction ($1 < n \leqq 2$), $N^{+} = 0$ or 1 and $N^{-} = -1, 0$ or 1.

At a shadow or reflection boundary one of the cotangent functions in the expression for D given by (6.33) becomes singular; the other three remain bounded. Even though the cotangent becomes singular, its product with the transition function can be shown to be bounded. The location of the boundary at which each cotangent becomes singular is presented in Table 6.1. Since discontinuity in the geometrical-optics field at a shadow or reflection boundary is compensated separately by one of the four terms in the diffraction coefficient, there is no problem in calculating the field when two boundaries are close to each other or coincide. The value of N^{+} or N^{-} at each boundary is included in Table 6.1 for convenience; these values remain unchanged in their respective transition regions unless kL is small.

The distance parameter L can be found by imposing the condition that the total field (the sum of the geometrical-optics field and the diffracted field) be continuous at shadow or reflection boundaries. One

Table 6.1. Behaviour of terms in the edge diffraction coefficient at shadow and reflection boundaries

	The cotangent is singular when	value of N at the boundary
$\cot\left(\frac{\pi+(\phi-\phi')}{2n}\right)$	$\phi = \phi' - \pi$, a SB surface $\phi = 0$ is shadowed	$N^{+} = 0$
$\cot\left(\frac{\pi-(\phi-\phi')}{2n}\right)$	$\phi = \phi' + \pi$, a SB surface $\phi = n\pi$ is shadowed	$N^{-} = 0$
$\cot\left(\frac{\pi+(\phi+\phi')}{2n}\right)$	$\phi = (2n-1)\pi - \phi'$, a RB reflection from surface $\phi = n\pi$	$N^{+} = 1$
$\cot\left(\frac{\pi-(\phi+\phi')}{2n}\right)$	$\phi = \pi - \phi'$, a RB reflection from surface $\phi = 0$	$N^{-} = 0$

obtains

$$L = \frac{s(\varrho_e^i + s)\,\varrho_1^i\,\varrho_2^i \sin^2\beta_0'}{\varrho_e^i(\varrho_1^i + s)(\varrho_2^i + s)}, \tag{6.40}$$

where ϱ_1^i, ϱ_2^i are the principal radii of curvature of the incident wavefront at Q_E, and ϱ_e^i is the radius of curvature of the incident wavefront in the edge fixed plane of incidence. Note that $\varrho = \varrho_e^i$ for the wedge.

Grazing incidence, where $\phi' = 0$ or $n\pi$ must be considered separately. In this case $D_s = 0$, and the expression for D_h given by (6.32) or (6.33) is multiplied by a factor of 1/2. The need for the factor of 1/2 may be seen by considering grazing incidence to be the limit of oblique incidence. At grazing incidence the incident and reflected fields merge, so that one half the total field propagating along the face of the wedge toward the edge is the incident field and the other half is the reflected field. Nevertheless, in this case it is clearly more convenient to regard the total field as the "incident" field. $D_s = 0$ implies that $E^d_{\beta_0}$ vanishes; however, as pointed out by KARP and KELLER [6.16], a higher-order term then becomes significant where $E^d_{\beta_0}$ is proportional to the normal derivative of $E^i_{\beta_0'}(Q_E)$. It can be shown for $\phi' = 0$ that

$$E^d_{\beta_0}(s) = \frac{1}{2}\,\frac{\partial E^i_{\beta_0'}(Q_E)}{\partial n} \cdot \frac{1}{jk\sin\beta_0}\,\frac{\partial}{\partial\phi'} D_s\bigg|_{\phi'=0} \sqrt{\frac{\varrho}{s(\varrho + s)}}\, e^{-jks}, \tag{6.41}$$

where D_s is given by (6.33). However, unlike (Ref. [16], Eq. (8)), the above expression may be used in the transition region adjacent to the shadow boundary at $\phi = \pi$. It was found to give accurate values of the diffracted field in the case of an infinitesimal slot (magnetic dipole) perpendicular to the edge of the wedge when the slot is only a quarter wavelength from the edge.

6.2.2. The General Edge Configuration

In the general case the surfaces forming the edge may be convex, concave or plane. Our solution is based of Keller's method of the canonical problem. The justification of the method is that high-frequency diffraction like high-frequency reflection is a local phenomenon, and locally one can approximate the curved edge geometry by a wedge, where the straight edge of the wedge is tangent to the curved edge at the point of incidence Q_E in Fig. 6.5 and its plane surfaces are tangent to the surfaces forming the curved edge. With these assumptions, the results for wedge diffraction can be applied directly to the curved edge problem. As we have just noted, there is an equivalent wedge associated with every curved edge structure, and so in generalizing the solution of the wedge, it is only necessary to modify the expressions for the distance parameter L, which appear in the arguments of the transition functions.

Thus the form of the dyadic diffraction coefficient is given by (6.31); the unit vectors and coordinates are shown in Fig. 6.5. It remains to determine the scalar diffraction coefficients. Outside the transition regions; these are given by (6.32).

The calculation of the caustic distance ϱ in (6.30) is not a trivial matter for curved edge diffraction. Employing differential geometry, it is shown in [6.8, 15] that

$$\frac{1}{\varrho} = \frac{1}{\varrho_e^i} - \frac{\hat{n}_e \cdot (\hat{s}' - \hat{s})}{a \sin^2 \beta_0'} \tag{6.42}$$

in which ϱ_e^i is the radius of curvature of the incident wavefront in the edge-fixed plane of incidence, which contains $\hat{s}'$ and $\hat{e}$ the unit vector tangent to the edge at Q_E; $\hat{n}_e$ is the unit vector normal to the edge at Q_E and directed away from the center of curvature; $\hat{s}'$ and $\hat{s}$ are unit vectors in the directions of incidence and diffraction, respectively, see Fig. 6.5a; a is the radius of curvature of the edge at Q_E, $a > 0$.

It is interesting to note that (6.42) like (6.17) and (6.18) has the same form as the elementary lens equation; here ϱ_e^i and ϱ correspond to the object and image distances, respectively.

As in the case of the wedge, the arguments of the transition functions are determined by imposing the condition that the total field be continuous at the shadow and reflection boundaries. It is found that

$$\begin{aligned} D_{\substack{s\\h}}(\phi, \phi'; \beta_0') = &\frac{-e^{-j\frac{\pi}{4}}}{2n\sqrt{2\pi k}\sin\beta_0'} \\ &\times \left[\cot\left(\frac{\pi + (\phi - \phi')}{2n}\right) F[kL^i a^+(\phi - \phi')] \right. \\ &+ \cot\left(\frac{\pi - (\phi - \phi')}{2n}\right) F[kL^i a^-(\phi - \phi')] \\ &\mp \left\{\cot\left(\frac{\pi + (\phi + \phi')}{2n}\right) F[kL^{ro} a^+(\phi + \phi')] \right. \\ &\left.\left. + \cot\left(\frac{\pi - (\phi + \phi')}{2n}\right) F[kL^{rn} a^-(\phi + \phi')]\right\}\right], \end{aligned} \tag{6.43}$$

$F(X)$, $a^{\pm}(\beta)$, $N^{\pm}$ being defined as before, and

$$L^{\mathrm{i}} = \frac{s(\varrho_{\mathrm{e}}^{\mathrm{i}} + s)\,\varrho_2^{\mathrm{i}}\varrho_1^{\mathrm{i}}\sin^2\beta_0'}{\varrho_{\mathrm{e}}^{\mathrm{i}}(\varrho_1^{\mathrm{i}} + s)(\varrho_2^{\mathrm{i}} + s)}, \tag{6.44}$$

$$L^{\mathrm{r}} = \frac{s(\varrho^{\mathrm{r}} + s)\,\varrho_2^{\mathrm{r}}\varrho_1^{\mathrm{r}}\sin^2\beta_0'}{\varrho^{\mathrm{r}}(\varrho_1^{\mathrm{r}} + s)(\varrho_2^{\mathrm{r}} + s)}, \tag{6.45}$$

where ϱ_1^{r} and ϱ_2^{r} are the principal radii of curvature of the reflected wavefront at $\mathrm{Q_E}$, and ϱ^{r} is the distance between the caustics of the diffracted ray in the direction of reflection. It may be found from (6.42) with $\hat{s} = \hat{s}' - 2(\hat{n}\cdot\hat{s}')\hat{n}$. The additional superscripts o and n on L in (6.43) denote that the radii of curvature (and caustic distance ϱ) are calculated at the reflection boundaries $\pi - \phi'$ and $(2n-1)\pi - \phi'$, respectively. In the far-zone where $s \gg \varrho$ and the principal radii of curvature ϱ_1 and ϱ_2 of the incident and reflected wavefronts at $\mathrm{Q_E}$, (6.44) and (6.45) simplify to

$$L = \frac{\varrho_1\varrho_2\sin^2\beta_0'}{\varrho}; \tag{6.46}$$

the appropriate superscripts are omitted here for the sake of simplicity.

Usually no more than one of the four transition functions is significantly different from one; furthermore the nature of the curved edge approximation is such that the first two terms within the brackets of (6.43) can be combined [6.8] to give

$$\frac{-2\sin\dfrac{\pi}{n}\,F\left[2kL^{\mathrm{i}}\cos^2\left(\dfrac{\phi-\phi'}{2}\right)\right]}{\cos\dfrac{\pi}{n} - \cos\left(\dfrac{\phi-\phi'}{n}\right)},$$

which considerably simplifies the calculation of the scalar diffraction coefficients.

In summary to calculate the diffraction from a curved edge, the scalar diffraction coefficients from (6.43) are substituted into (6.31), and the resulting dyadic diffraction coefficient is substituted into (6.30). The caustic distance ϱ is calculated from (6.42). In matrix notation

$$\begin{bmatrix} E_{\beta_0}^{\mathrm{d}} \\ E_{\phi}^{\mathrm{d}} \end{bmatrix} = \begin{bmatrix} -D_{\mathrm{s}} & 0 \\ 0 & -D_{\mathrm{h}} \end{bmatrix} \begin{bmatrix} E_{\beta_0'}^{\mathrm{i}} \\ E_{\phi'}^{\mathrm{i}} \end{bmatrix} \sqrt{\frac{\varrho}{s(\varrho+s)}}\,\mathrm{e}^{-jks}. \tag{6.47}$$

The present treatment does not include the modification of the edge diffracted field which occurs when either the incident or diffracted ray grazes the surface. The angle between these rays and the surface should exceed $(ka_i)^{-1/3}$, where a_i is the radius of curvature of the surface at Q_E in the direction of the incident (or diffracted) ray. Also the present treatment does not include the effect of surface rays excited at the edge.

6.2.3. Higher-Order Edges

The preceding discussion has been restricted to ordinary edges where the unit normal vector to the surface is discontinuous. However, in the case of higher-order edges, where some j-th derivative of the surface has a jump discontinuity (while all lower derivatives are continuous), it has been shown [6.8] that the dyadic diffraction coefficient has the same form as in (6.31). Also the dyadic diffraction coefficient for the scattering from thin, curved wires has this form too.

Recently, KELLER and KAMINETZKY [6.17] and SENIOR [6.18] have obtained expressions for the scalar diffraction coefficients in the case of diffraction by an edge formed by a discontinuity in surface curvature and SENIOR has given the dyadic (or matrix) diffraction coefficient in an edge-fixed coordinate system. When transformed to the ray-fixed coordinate system, Senior's expression for the diffracted field reduces to the form in (6.30) with $\underset{\sim}{D}$ given by (6.31). KELLER and KAMINETZKY [6.17] also have given expressions for the scalar diffraction coefficients in the case of higher-order edges.

6.3. Diffraction by a Vertex

The vertex or corner is a point caustic of the diffracted rays, from (6.28) and the discussion following, the expression for the electric field of the vertex diffracted ray is

$$E^d(s) = E^i(Q_v) \cdot \underset{\sim}{D}(\theta, \phi; \theta', \phi') \frac{e^{-jks}}{s}. \tag{6.48}$$

From dimensional considerations similar to those applied to the wedge, this diffraction coefficient must vary as k^{-1}, which means that outside its transitions regions the vertex-diffracted field is in general significantly weaker than the edge-diffracted field. Very little work has been done on the high-frequency diffraction by vertices; it is a complicated, difficult subject, and there are a variety of such geometries to consider. Some results for blunt vertices may be obtained from [6.17], and the diffraction coefficient for the vertex of a cone in some special cases may be obtained from [6.19, 20].

6.4. Surface Diffraction

When an incident ray strikes a smooth, curved perfectly-conducting surface at grazing incidence, i.e., at the shadow boundary, a part of its energy is diffracted into the shadow region. Let us consider the field radiated by the source 0 and observed at P in the shadow region, as shown in Fig. 6.6. Applying the generalized Fermat's principle, the distance $0Q_1Q_2P$ is the shortest distance between 0 and P which does not penetrate the surface. In detail, a ray incident on the shadow boundary

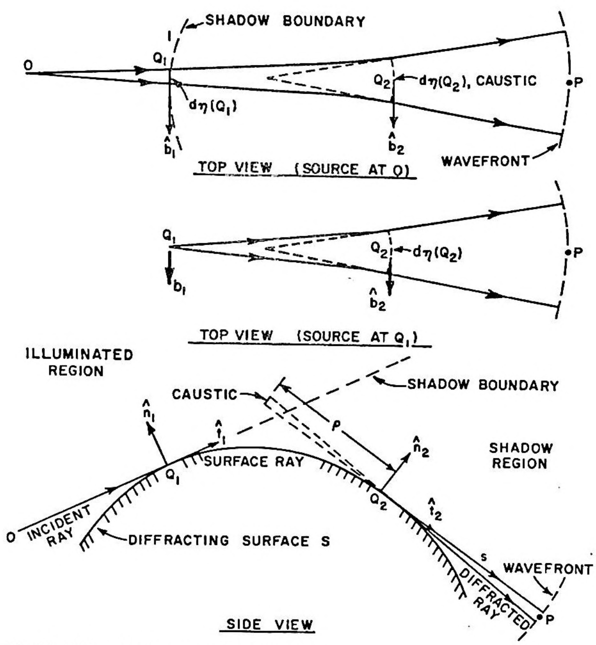

Fig. 6.6. Diffraction by a smooth convex surface

at Q_1 divides; one part of the incident energy continues straight on as predicted by geometrical optics and a second part follows the surface S into the shadow region as a surface ray, which sheds diffracted rays tangentially as it propagates. It follows from this extension of Fermat's principle that the incident and diffracted rays are tangent to S and to the surface ray at Q_1 and Q_2, respectively, and that the surface ray is the shortest distance between Q_1 and Q_2 on S, i.e., the surface ray is a geodesic curve. The former statement is referred to as the law of surface diffraction, and it also may be deduced from the requirement that the incident and diffracted fields are phase matched to the surface ray field at Q_1 and Q_2. At Q_1 let $\hat{t}_1$ be the unit vector in direction of incidence, $\hat{n}_1$ be the unit vector normal to S and $\hat{b}_1 = \hat{t}_1 \times \hat{n}_1$; at Q_2 let a similar set of unit vectors be defined with $\hat{t}_2$ in the direction of the diffracted ray.

A second configuration of interest occurs when the source is positioned on the surface, say at Q_1. This configuration is relevant to the radiation from an aperture in S, where the equivalent source is an infinitesimal magnetic current moment (magnetic dipole)

$$d\boldsymbol{p}_m(Q_1) = \boldsymbol{E}(Q_1) \times \hat{n}_1 \, da \tag{6.49}$$

in which $\boldsymbol{E}$ is the aperture electric field, and da is an area element of the aperture. Another type of source which may be positioned at Q_1 is the normally-directed electric current dipole. According to the generalized Fermat's principle, the ray trajectory from these sources to P is the curve $Q_1 Q_2 P$ mentioned previously.

The discussion to follow is devoted to methods of calculating the field in the shadow and transition regions of a convex, perfectly-conducting surface. Deep in the illuminated region the field directly radiated from the source is found by geometrical optics. Expressions for this field are well known and will not be repeated here. When the source is not on the surface the reflected field may be calculated from (6.14), (6.16)–(6.19).

6.4.1. The Shadow Region

From Fig. 6.6 it is seen that Q_2 is a caustic of the diffracted field. There is a second caustic at a distance ϱ from this caustic. As noted earlier, the diffracted field at P is given by (6.25), where it is convenient to let

$$\boldsymbol{C} = \hat{n}_2 C_n + \hat{b}_2 C_b \tag{6.50}$$

in this case. The C_n, C_b are proportional to the surface ray field incident at Q_2; however, as in the case of edge diffraction, the precise relationship (like much of the development to follow) is deduced from the asymptotic

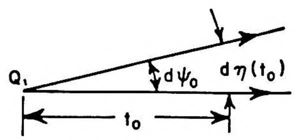

Fig. 6.7. Surface ray configuration close to a point source

solution of certain canonical problems, which will be described later. To simplify the discussion, it is assumed that the surface rays are torsionless, i.e., $\hat{b}$ does not change direction along the surface ray.

From the canonical problems it is found that the surface ray field is composed of infinitely many modes which propagate independently of each other along a torsionless path. Let the field associated with one of these modes be

$$a(t) = A(t)\, e^{j(\phi_0 - kt)}, \tag{6.51}$$

where t is the distance along the surface ray measured from Q_1, ϕ_0 is the phase at Q_1, and initially one assumes that $A(t)$ is real.

The surface ray sheds rays tangentially as it propagates along a geodesic on the curved surface; hence energy is continuously lost from the surface ray field, and the field of each mode is attenuated. In addition, it is assumed that the energy flux between adjacent surface rays is conserved. This may be expressed by

$$d/dt(A^2\, d\eta) = -2\alpha(A^2\, d\eta), \tag{6.52}$$

where α is the attenuation constant for the surface ray mode in question. The above equation is readily integrated between t_0 and t to give

$$a(t) = a(t_0)\sqrt{\frac{d\eta(t_0)}{d\eta(t)}}\exp\left\{-\left[jk(t-t_0) + \int_{t_0}^{t}\alpha(t')\,dt'\right]\right\}. \tag{6.53}$$

The attenuation constant is a function of t' because it depends on the local curvature of the surface.

Equation (6.53) must be modified when there is a caustic due to a point source on the surface at Q_1, where $t = 0$. For t_0 small $d\eta(t_0) = t_0\, d\psi_0$ is the angle between adjacent surface rays, see Fig. 6.7. Moreover, $a(t)$ must be independent of t_0; hence $\lim a(t_0)\sqrt{t_0}$ exists as $t_0 \to 0$ and we define it to be K. It follows then that

$$a(t) = K\sqrt{\frac{d\psi_0}{d\eta}}\exp\left\{-\left[jkt + \int_0^t \alpha(t')\,dt'\right]\right\}. \tag{6.54}$$

The constant K is proportional to the strength of the source at Q_1.

For the source at 0 removed from the boundary surface, the incident field at Q_1 may be resolved into normal and binormal components, which induce hard (h) and soft (s) type surface ray modes, respectively. The normal derivative of the field at S vanishes for the hard boundary condition[3], and the field at S vanishes for the soft boundary condition. Thus

$$\hat{n}_1 \cdot E^{\mathrm{i}}(1)\, D_p^{\mathrm{h}}(1) = a_p^{\mathrm{h}}(1), \tag{6.55a}$$

$$\hat{b}_1 \cdot E^{\mathrm{i}}(1)\, D_p^{\mathrm{s}}(1) = a_p^{\mathrm{s}}(1), \tag{6.55b}$$

where the constant of proportionality D is the surface diffraction coefficient, the superscript h(s) denotes a quantity associated with the hard (soft) boundary condition, the subscript p denotes the pth surface ray mode and Q_1 and Q_2 are replaced by 1 and 2 for the sake of notational economy.

At Q_2 the components of C are linearly related to the surface ray field:

$$\sum_p a_p^{\mathrm{h}}(2)\, D_p^{\mathrm{h}}(2) = C_n, \tag{6.56a}$$

$$\sum_p a_p^{\mathrm{s}}(2)\, D_p^{\mathrm{s}}(2) = C_b. \tag{6.56b}$$

Now substituting (6.56) into (6.50) and (6.25), noting that $a_p(1)$ and $a_p(2)$ are related by (6.53) and employing (6.55), one obtains

$$E^{\mathrm{d}}(P) = E^{\mathrm{i}}(1)\cdot[\hat{n}_1\hat{n}_2 F + \hat{b}_1\hat{b}_2 G]\sqrt{\frac{\varrho}{s(\varrho+s)}}\,\mathrm{e}^{-jks} \tag{6.57}$$

in which

$$F = \mathrm{e}^{-jkt}\sqrt{\frac{d\eta_1}{d\eta_2}}\sum_{p=1}^{\infty} D_p^{\mathrm{h}}(1)\, D_p^{\mathrm{h}}(2)\;T_p^{\mathrm{h}} \tag{6.58}$$

[3] This approximation of the hard boundary condition for electromagnetic waves is adequate for the present discussion. A more complete treatment is given later.

and G has the same form as F except that the superscript h is replaced by s. Here t is the distance between Q_1 and Q_2 along the surface ray, and we have set

$$\exp\left[-\int_0^t \alpha_p^{\mathrm{h}}(t')\,dt'\right] = T_p^{\mathrm{h}} \tag{6.59}$$

for the sake of notational brevity. If the reciprocity principle is to be satisfied, $D_p(1)$ must have the same functional dependence as $D_p(2)$, i.e., if a source at 0 is to produce the same field at P as a source at P produces at 0. It is apparent that the bracketed quantity in (6.57) serves as a generalized diffraction coefficient for the convex surface, analogous to (6.31) for the edge.

If S is a closed surface, a surface ray initiated at Q_1 may encircle S an infinite number of times. The length of the surface ray path for the lth encirclement is $t + lT$ with T the length of the closed path. These multiply-encircling rays can be summed to contribute

$$1 - \exp\left\{-\left(jkT + \int_0^T \alpha_p(t')\,dt'\right)\right\}$$

to the denominator of the expression for the diffracted field.

If the source is on the surface at Q_1, one still employs (6.56), (6.50), and (6.25); however in this case $a_p(2)$ is related to $a_p(1)$ by (6.54), and at Q_1

$$\frac{-jk}{4\pi}\,d\boldsymbol{p}_m \cdot \hat{b}_1\, L_p^{\mathrm{h}} = K_p^{\mathrm{h}}, \tag{6.60a}$$

$$\frac{-jk}{4\pi}\,d\boldsymbol{p}_m \cdot \hat{t}_1\, L_p^{\mathrm{s}} = K_p^{\mathrm{s}}, \tag{6.60b}$$

where the constants of proportionality are referred to as launching coefficients. It follows then that

$$dE^{\mathrm{d}}(P) = d\boldsymbol{p}_m \cdot [\hat{b}_1 \hat{n}_2 F_s + \hat{t}_1 \hat{b}_2 G_s] \sqrt{\frac{\varrho}{s(\varrho + s)}}\, \mathrm{e}^{-jks} \tag{6.61}$$

in which

$$F_s = \frac{-jk\mathrm{e}^{-jkt}}{4\pi} \sqrt{\frac{1}{\varrho}\frac{d\psi_1}{d\psi_2}} \sum_{p=1}^{\infty} L_p^{\mathrm{h}}(1)\, D_p^{\mathrm{h}}(2)\, T_p^{\mathrm{h}} \tag{6.62}$$

and G_s has the same form as F_s except that the superscript h is replaced by s. In (6.54) $d\psi_0$ has been replaced $d\psi_1$, and $d\eta = d\eta_2 = \varrho\, d\psi_2$. $E^d(P)$ is calculated by integrating over the aperture in question.

At first glance it may seem that the field on S can be calculated directly from the surface ray field. However, the surface ray field is not a physically observable field; as a matter of fact, it does not have the dimensions of an electric or magnetic field, as will be seen when the expressions for D_p are given. Thus in (6.56) the surface ray field merely serves as a transfer function between the incident field at Q_1 and the diffracted field at Q_2. However, both the surface ray field and the field on the surface vary with respect to t in the same manner, which makes it possible to calculate the magnetic field at Q_2 on the perfectly-conducting surface by introducing attachment coefficients A_p in the place of diffraction coefficients at Q_2.

Thus for a source at 0

$$H(Q_2) = Y_c E^i \cdot [\hat{n}_1 \hat{b}_2 \mathscr{F} + \hat{b}_1 \hat{t}_2 \mathscr{G}], \tag{6.63}$$

and for a source at Q_1

$$dH(Q_2) = Y_c\, dp_m \cdot [\hat{b}_1 \hat{b}_2 \mathscr{F}_s + \hat{t}_1 \hat{t}_2 \mathscr{G}_s], \tag{6.64}$$

where

$$\mathscr{F} = e^{-jkt} \sqrt{\frac{d\eta_1}{d\eta_2}} \sum_{p=1}^{\infty} D_p^h(1)\, A_p^h(2)\, T_p^h \tag{6.65a}$$

$$\mathscr{F}_s = \frac{-jke^{-jkt}}{4\pi} \sqrt{\frac{1}{\varrho} \frac{d\psi_1}{d\psi_2}} \sum_{p=1}^{\infty} L_p^h(1)\, A_p^h(2)\, T_p^h \tag{6.65b}$$

$$Y_c = 1/Z_c,$$

and $\mathscr{G}$ and $\mathscr{G}_s$ have the same form as $\mathscr{F}$ and $\mathscr{F}_s$, respectively, except that the superscript h is replaced by s.

Employing reciprocity it is found that

$$A_p^h = L_p^h \tag{6.66a}$$

and

$$A_p^s = -L_p^s, \tag{6.66b}$$

which is not surprising when one recalls that the diffraction coefficient is the same for the excitation of a surface ray mode and the radiation from a surface ray mode.

If the surface source at Q_1 is an electric current dipole $P_e = Il\hat{n}_1$,

$$E(P) = \hat{n}_2 Z_c I l F_s \sqrt{\frac{\varrho}{s(\varrho+s)}}\, e^{-jks}, \tag{6.67}$$

with F_s given by (6.62), and the magnetic field induced on S is

$$H(Q_2) = \hat{b}_2 I l \mathscr{F}_s \tag{6.68}$$

with $\mathscr{F}_s$ given by (6.65b).

In the case of simple surfaces such as the spherical surface, the cylindrical surface, the conical surface and the plane surface, the geodesics are known and they are easy to describe; otherwise they can be found from the differential equations for geodesic paths, which is a formidable but straight forward exercise, see [6.26]. Calculating $d\eta_1$, $d\eta_2$, $d\psi_1$, $d\psi_2$ and ϱ is a matter of differential geometry involving the rays and the surface; this is discussed in [6.21, 26]. In the paragraphs to follow expressions will be given for the diffraction coefficients, launching coefficients and attenuation constants.

6.4.2. The Parameters

The diffraction coefficients, launching coefficients, and attenuation constants depend on the local geometry of the surface, the wave number k, and the nature of the surface, as described by the boundary conditions. KELLER and LEVY [6.21] have given the first-order terms in the expressions for the diffraction coefficients and attenuation constants. However, before we present their results, it is desirable to examine further the terms "soft" and "hard" boundary conditions.

This terminology is borrowed from acoustics. A soft boundary is one where the pressure field vanishes at the surface; it is also referred to as a Dirichlet boundary. On the other hand, a hard boundary is one where the normal derivative of the pressure field vanishes at the surface; this is also referred to as a Neumann boundary. Two types of surface ray modes have been assumed. For one type the electric field is in the binormal direction so that $E_p = \hat{b} E_p$, and for the other, the magnetic field is in the binormal direction so that $H_p = \hat{b} H_p$, and there is a normally-directed electric field $\hat{n} \cdot E_p$. The binormally directed electric field clearly satisfies a soft or Dirichlet boundary condition at the surface, whereas the binormally-directed magnetic field satisfies the boundary condition

$$\frac{\partial H}{\partial n} + \left(\frac{1}{h_b}\frac{\partial h_b}{\partial n}\right) H = 0, \tag{6.69}$$

in which h_b is the metrical coefficient associated with the unit vector $\hat{b}$. The above boundary condition describes what we will refer to as a hard EM boundary. At high frequencies the second term is relatively small, so that the surface ray magnetic field satisfies a hard or Neumann boundary condition to a first approximation. Also (6.69) reduces to the hard boundary condition in the case of cylindrical surfaces where $h_b = 1$. These observations concerning the boundary conditions are of importance in the paragraphs to follow.

Let ϱ_g ne the radius of curvature of the surface along which the surface ray is propagating in the plane containing the normal to the surface and the tangent to the surface ray. As mentioned earlier, KELLER and LEVY [6.21] have used first-order asymptotic solutions for the diffraction of acoustic (scalar) and electromagnetic waves to deduce the attenuation constants and diffraction coefficients. For these canonical problems $\varrho_g = a$, a constant. According to KELLER and LEVY

$$\alpha^{s}_{0p} = \frac{1}{a}\left(\frac{ka}{2}\right)^{1/3} q_p\, e^{j\frac{\pi}{6}}, \tag{6.70}$$

$$[D^{s}_{0p}]^2 = \frac{e^{-j\frac{\pi}{12}}}{2^{5/6}\pi^{1/2}(ka)^{1/6}} \frac{a^{1/2}}{[\mathrm{Ai}'(-q_p)]^2} \tag{6.71}$$

for the soft surface, and

$$\alpha^{h}_{0p} = \frac{1}{a}\left(\frac{ka}{2}\right)^{1/3} q_p\, e^{j\frac{\pi}{6}} \tag{6.72}$$

$$[D^{h}_{0p}]^2 = \frac{e^{-j\frac{\pi}{12}}}{2^{5/6}\pi^{1/2}(ka)^{1/6}} \frac{1}{q_p} \frac{a^{1/2}}{[\mathrm{Ai}(-q_p)]^2} \tag{6.73}$$

for the hard surface, where the Miller-type Airy function is given by

$$\mathrm{Ai}(-x) = \frac{1}{\pi}\int_0^\infty \cos\left(\tfrac{1}{3}t^3 - xt\right) dt\,,$$

$$\mathrm{Ai}(-q_p) = 0\,,$$

$$\mathrm{Ai}'(-q_p) = 0\,,$$

and the prime denotes differentiation with respect to the argument of the function.

Table 6.2. Diffraction coefficients and attenuation constants for the curved surface

Surface	Square of diffraction coefficient $D_p^2 = $ (Column A) · (Column B)	
	A. Keller's result	B. Correction terms
Soft acoustic and soft EM	$\dfrac{\pi^{-1/2}2^{-5/6}\varrho_g^{1/3}\mathrm{e}^{-j\pi/12}}{k^{1/6}(\mathrm{Ai}'(-q_p))^2}$	$1+\left(\dfrac{2}{k\varrho_g}\right)^{2/3} q_p\left(\dfrac{1}{30}+\dfrac{\varrho_g}{4\varrho_{tn}}+\cdots\right)$
Hard acoustic	$\dfrac{\pi^{-1/2}2^{-5/6}\varrho_g^{1/3}\mathrm{e}^{-j\pi/12}}{k^{1/6}q_p(\mathrm{Ai}(-q_p))^2}$	$1+\left(\dfrac{2}{k\varrho_g}\right)^{2/3}\left(q_p\left(\dfrac{1}{30}+\dfrac{\varrho_g}{4\varrho_{tn}}+\cdots\right) - \dfrac{1}{q_p^2}\left(\dfrac{1}{10}+\dfrac{\varrho_g}{4\varrho_{tn}}+\cdots\right)\right)\mathrm{e}^{-j\pi/}$
Hard EM		$1+\left(\dfrac{2}{k\varrho_g}\right)^{2/3}\left(q_p\left(\dfrac{1}{30}+\dfrac{\varrho_g}{4\varrho_{tn}}+\cdots\right) - \dfrac{1}{q_p^2}\left(\dfrac{1}{10}-\dfrac{\varrho_g}{4\varrho_{tn}}+\cdots\right)\right)\mathrm{e}^{-j\pi/}$

ϱ_g = radius of curvature along the geodesic
ϱ_{tn} = radius of curvature perpendicular to the geodesic (transverse curve)
Dots indicate differentiation with respect to the arc length variable

VOLTMER [6.25] employing the same canonical problems as KELLER and LEVY, obtained attenuation constants and diffraction coefficients of improved accuracy by retaining higher-order terms in the asymptotic solutions. Voltmer's corrections to the attenuation constants and diffraction coefficients are of order $(2/ka)^{2/3}$.

The first-order approximations given by (6.70)–(6.73) do not depend on whether the surface is cylindrical or spherical or on whether the wave is acoustic or electromagnetic; however this is no longer the case with the more accurate formulas. An explanation of these second-order differences is best accomplished by examining the high-frequency diffraction from a more general surface, i.e., a surface of variable curvature along the ray path or of arbitrary curvature transverse to the ray path.

KELLER and LEVY [6.22], FRANZ and KLANTE [6.23], HONG [6.24], and VOLTMER [6.25] have considered the high-frequency diffraction by general convex surfaces. HONG has obtained asymptotic solutions to the integral equations for the plane wave diffraction by a hard acoustic surface and the plane wave diffraction by a hard EM boundary. VOLTMER has extended this work to soft boundaries, which are the same for acoustic and EM waves, as we have noted. The solutions were carried out to second order, and they are functions not only of ϱ_g, the radius of

enuation constant = (Column C) · (Column D)		Zeroes of the Airy function $\mathrm{Ai}(-q_p) = 0$ $q_1 = 2.33811$ $q_2 = 4.08795$ $\mathrm{Ai}'(-q_1) = .70121$ $\mathrm{Ai}'(-q_2) = -.80311$
Keller's result	D. Correction terms	
$e^{j\pi/6}\left(\frac{k\varrho_g}{2}\right)^{1/3}$	$1 + \left(\frac{2}{k\varrho_g}\right)^{2/3} q_p\left(\frac{1}{60} - \frac{2}{45}\varrho_g\ddot{\varrho}_g + \frac{4}{135}\dot{\varrho}_g^2\right) e^{-j\pi/3}$	
$e^{j\pi/6}\left(\frac{k\varrho_g}{2}\right)^{1/3}$	$1 + \left(\frac{2}{k\varrho_g}\right)^{2/3}\left(q_p\left(\frac{1}{60} - \frac{2}{45}\varrho_g\ddot{\varrho}_g + \frac{4}{135}\dot{\varrho}_g^2\right) + \frac{1}{q_p^2}\left(\frac{1}{10} + \frac{\varrho_g}{4\varrho_{tn}} - \frac{\varrho_g\ddot{\varrho}_g}{60} + \frac{\dot{\varrho}_g^2}{90}\right)\right) e^{-j\pi/3}$	Zeroes of the derivative of the Airy function $\mathrm{Ai}'(-q_p) = 0$ $q_1 = 1.01879$ $q_2 = 3.24820$ $\mathrm{Ai}(-q_1 = .53566$ $\mathrm{Ai}(-q_2) = -.41902$
	$1 + \left(\frac{2}{k\varrho_g}\right)^{2/3}\left(q_p\left(\frac{1}{60} - \frac{2}{45}\varrho_g\ddot{\varrho}_g + \frac{4}{135}\dot{\varrho}_g^2\right) + \frac{1}{q_p^2}\left(\frac{1}{10} - \frac{\varrho_g}{4\varrho_{tn}} - \frac{\varrho_g\ddot{\varrho}_g}{60} + \frac{\dot{\varrho}_g^2}{90}\right)\right) e^{-j\pi/3}$	

curvature of the surface with respect to arc length along the ray trajectory, but also $\dot{\varrho}_g$, $\ddot{\varrho}_g$, and ϱ_{tn}, where the dot denotes a derivative with respect to arc length along the ray trajectory, and ϱ_{tn} is the radius of curvature of the surface in the direction of the binormal to the ray. Expressions for the attenuation constants are evident from the solutions; these are tabulated in Columns C and D of Table 6.2. On the other hand, complete expressions for the diffraction coefficients cannot be obtained from these solutions, because $\dot{\varrho}_g$ is assumed to be zero at the point of incidence on the surface, where the diffraction coefficient is evaluated. This condition was imposed to simplify the pertinent integral equations. The diffraction coefficients (more precisely, the diffraction coefficients squared) are given in Columns A and B of Table 6.2. The incomplete portion of the second-order term is indicated by (...); it is a function of $\dot{\varrho}_g$ and $\ddot{\varrho}_g$[4]. In deriving these results it is assumed that $\varrho_g/\varrho_{tn} < 1$: furthermore it is assumed that the surface rays have no torsion.

It is believed that the attenuation constants and diffraction coefficients listed in Table 6.2 are the best available at present and that they are adequate for most calculations, even though the expressions for the

[4] The $\dot{\varrho}_g$ and $\ddot{\varrho}_g$ terms in the diffraction coefficient will be the subject of a future investigation.

diffraction coefficients are not complete to second order. The improved attenuation constants are very important, because of the sensitivity of numerical calculations to errors in these parameters, particularly in the deep shadow region; corresponding errors in the diffraction coefficient are clearly less important to numerical accuracy.

The launching coefficients have been defined in (6.60). To determine the launching coefficients the radiation from a magnetic current moment on a perfectly-conducting sphere and the radiation from magnetic current line sources on cylindrical surfaces have been analyzed [6.27]. From the asymptotic solution of these canonical problems and their ray-optical interpretation it is found that for both cylindrical and spherical surfaces

$$L_p^s = -\left(jk\frac{\pi}{2}\right)^{1/2} H_{\nu_p}^{(2)\prime}(ka)\, D_p^s ,$$

$$L_p^h = -j\left(jk\frac{\pi}{2}\right)^{1/2} H_{\nu_p}^{(2)}(ka)\, D_p^h ,$$

where ν_p are the zeroes of the Hankel function in the first equation and the zeroes of the derivative of the Hankel function in the second equation. It is apparent that the relationship of the launching coefficient to the diffraction coefficient does not depend on the surface curvature transverse to the ray direction. For this reason, one may assume that

$$L_p^s = e^{-j\frac{\pi}{12}}(2\pi k)^{1/2}\left(\frac{2}{k\varrho_g}\right)^{2/3} \cdot \mathrm{Ai}'(-q_p)\left[1-\left(\frac{2}{k\varrho_g}\right)^{2/3}\frac{q_p}{15}\, e^{j\frac{2\pi}{3}}\right] D_p^s , \tag{6.74}$$

$$L_p^h = e^{j\frac{\pi}{12}}(2\pi k)^{1/2}\left(\frac{2}{k\varrho_g}\right)^{1/3} \cdot \mathrm{Ai}(-q_p)\left[1+\left(\frac{2}{k\varrho_g}\right)^{2/3}\frac{q_p}{15}\, e^{j\frac{2\pi}{3}}\right] D_p^h . \tag{6.75}$$

These expressions for the launching coefficients, where D_p^s and D_p^h are obtained from Table 6.2, are the best available at present. It would be desirable to solve a canonical problem where the magnetic current moment or line source is on a surface of variable curvature as a further check. The attachment coefficients follow from the above equations and (6.66).

From Table 6.2 it is seen that the real part of $\alpha_p^h <$ the real part of α_p^s so that T_p^h is exponentially larger than T_p^s and the F-type functions are exponentially larger than the G-type functions. Thus in the shadow region, the contributions from the latter functions are important only when $E^i(1)$ is nearly parallel to $\hat{b}_1$ or dp_m is nearly parallel to $\hat{t}_1$. Furthermore from examples involving a cylindrical geometry, it has been found that the dominant F-type functions are independent of torsion to a first-order approximation; however this is not the case for G_s, $\mathcal{G}$, and $\mathcal{G}_s$. Torsion appears to be a second-order effect, which is important mostly when accuracy is required in the deep shadow region.

6.4.3. Transition Regions

The series representations are rapidly convergent when the field point is deep in the shadow region. Usually only the first few terms are required to achieve reasonable accuracy, when the radii of curvature of the surface are larger than a wavelength or so. However as the field point Q_2 approaches close to Q_1 and more terms must be added to maintain accuracy, it is then no longer desirable to treat the excitation, propagation and diffraction of the different surface ray modes separately. As a result, the series representations are replaced by integral representations, and these are found to be proportional to Fock-type functions. When the source is on the surface the angular extent of the transition region from the shadow boundary is roughly $(k\varrho_g)^{-1/3}$; when the source is removed from the surface it is more nearly $(k\varrho_g/2)^{-1/3}$.

In contrast with the deep shadow region a first-order asymptotic approximation is usually adequate for the transition region. In numerous calculations it was found that curves obtained from the expressions for the transition region joined smoothly with those obtained from expressions for the shadow region.

In describing the fields in the transition region, we employ the Fock-type Airy functions

$$w_1(\tau) = \frac{1}{\sqrt{\pi}} \int_{\Gamma_1} e^{\tau z - z^3/3}\, dz \tag{6.76}$$

and $w_2(\tau)$, which has the same form as $w_1(\tau)$ except that the contour of integration is Γ_2; these contours of integration are shown in Fig. 6.8. In the expressions to follow it will be convenient to use

$$\xi = \int_0^t \frac{1}{\varrho_g} \left(\frac{k\varrho_g}{2}\right)^{1/3} dt'. \tag{6.77}$$

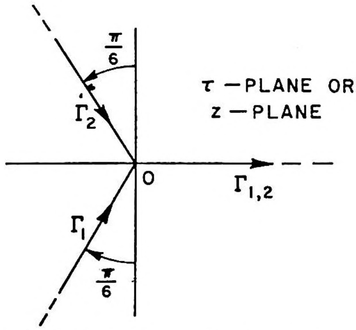

Fig. 6.8. Contours of integration for the Airy and Fock functions

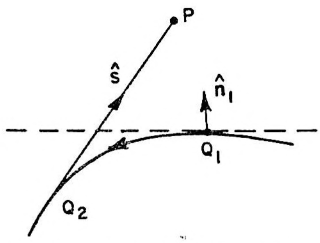

Fig. 6.9. A pseudo-ray system for calculating the field in the illuminated part of the transition region

In terms of ξ

$$T_p^h = e^{-j\xi\tau_p}. \quad \text{and} \quad T_p^s = e^{-j\xi\tau_p}$$

to first order, where $\tau_p = q_p \exp(-j\pi/3)$ and $\tau_p = q_p \exp(-j\pi/3)$.

When the field point is in the shadow region $\xi, t > 0$ and when the field point is in the illuminated region $\xi, t < 0$. In the illuminated portion of the transition region, one visualizes the surface ray as travelling from Q_1 to Q_2, where it sheds tangentially back toward P, as shown in Fig. 6.9. The ray path $Q_1 Q_2 P$ does not obey the generalized Fermat's principle and therefore it is a pseudo-ray system, but it does serve as a useful coordinate system to calculate the field at P in the illuminated part of the transition region. Note that the surface ray divergence factors $\sqrt{d\eta_1/d\eta_2}$ and $\sqrt{d\psi_1/d\psi_2}$ are equal to one in this region.

As in the deep region, the expressions for the field in the transition region may be deduced from the solutions of the canonical problems for this region. On the other hand, recognizing the GTD solution for the deep shadow region as a residue series, it is sometimes possible to infer the integral representation from which it follows. However, this is a risky procedure and it appears to yield useful results only when the source is on the surface.

In the transition region

$$\sum_{p=1}^{\infty} L_p^{\mathrm{h}}(1)\, D_2^{\mathrm{h}}(2)\, T_p^{\mathrm{h}} \quad \text{is replaced by} \qquad g(\xi) \times \begin{cases} 1, & t \leqq 0 \\ x, & t \geqq 0 \end{cases}, \tag{6.78}$$

$$\sum_{p=1}^{\infty} L_p^{\mathrm{s}}(1)\, D_p^{\mathrm{s}}(2)\, T_p^{\mathrm{s}} \quad \text{is replaced by} \qquad -j\tilde{g}(\xi) \times \begin{cases} -\hat{n}_1 \cdot \hat{s}/\xi, & t \leqq 0 \\ x/m, & t \geqq 0 \end{cases}, \tag{6.79}$$

$$\sum_{p=1}^{\infty} L_p^{\mathrm{h}}(1)\, A_p^{\mathrm{h}}(2)\, T_p^{\mathrm{h}} \quad \text{is replaced by} \qquad \left(\frac{jk}{2}\right)^{1/2} (mx)^{-1}\, \psi(\xi), \quad t > 0, \tag{6.80a}$$

$$\sum_{p=1}^{\infty} L_p^{\mathrm{s}}(1)\, A_p^{\mathrm{s}}(2)\, T_p^{\mathrm{s}} \quad \text{is replaced by} \qquad -\left(\frac{jk}{2}\right)^{1/2} (mx)^{-3}\, \tilde{\psi}(\xi), \quad t > 0, \tag{6.80b}$$

where

$$\tilde{g}(\xi) = \frac{1}{\sqrt{\pi}} \int_{\Gamma_1} \frac{e^{-j\xi\tau}}{w_2(\tau)}\, d\tau,$$

$$\psi(\xi) = \frac{1}{\sqrt{\pi}} \int_{\Gamma_1} \frac{w_2(\tau)}{w_2'(\tau)}\, e^{-j\xi\tau}\, d\tau,$$

and

$$m = \left[\frac{k\varrho_g(1)}{2}\right]^{1/3},$$

$$x = \left[\frac{\varrho_g(2)}{\varrho_g(1)}\right]^{1/6}.$$

The function $g(\xi)$ has the same form as $\tilde{g}(\xi)$ except that $w_2(\tau)$ in the integrand is replaced by its derivative; moreover $\tilde{\psi}(\xi)$ follows from $\psi(\xi)$ when w_2'/w_2 is substituted for w_2/w_2'. The Fock-type functions above have been described and tabulated by LOGAN [6.28]; they are also briefly described in (Ref. [6.9], Section 1.3.3).

The expressions for the transition regions in (6.78) and (6.79) have been found to be very useful. Patterns calculated from them blend well with those calculated from geometrical optics deep in the illuminated region and from the surface ray modes in the shadow region [6.27]. On the other hand, (6.80a) and (6.80b) appear to be of limited value because the GTD approximation precludes Q_2 from being closer to Q_1 than a half wavelength or so. Moreover when the distance between Q_1 and Q_2 is small compared with ϱ_g, the currents or mutual coupling can be calculated with reasonable accuracy by assuming the surface is plane.

When the GTD solution involves a field reflected from a curved surface, the geometrical-optics representation of the reflected field is usually the greatest source of error. Furthermore the behavior of the field in the transition region adjacent to the shadow boundary is more complex than in the case of edge diffraction; this is particularly true in the illuminated part, where the solution should match the geometrical-optics approximation of the total field.

WAIT and CONDA [6.29] have obtained expressions for the field diffracted by a circular cylinder or sphere near the shadow boundary using a method based on the earlier work of FOCK [6.30] and GORIAINOV [6.31]. Their solution has been adapted (with slight modification) to the GTD format used here, with the result that for a surface whose ϱ_g is nearly constant in the transition region.

$$\sum_{p=1}^{\infty} D_p^{\mathrm{h}}(1)\, D_p^{\mathrm{h}}(2)\, T_p^{\mathrm{h}}$$

is replaced by (6.81)

$$D(x) - \left(\frac{2}{k}\right)^{1/2} m\, G(\xi)$$

with

$$D(x) = \sqrt{\frac{L}{\pi}}\, e^{j\left(\frac{\pi}{4}+x\right)}\, \operatorname{sgn}(\delta) \int_{|\sqrt{x}|}^{\infty} e^{-j\tau^2}\, d\tau\,,$$

$$x = 2kL\left(\frac{\delta}{2}\right)^2,$$

$$\xi = m\delta\,,$$

$$\delta = -\sin^{-1} \hat{n}_1 \cdot \hat{t}_2\,,$$

$$L = \frac{ss'}{s+s'}\,,$$

for cylindrical and spherical waves normally incident on the shadow boundary. The quantities s' and s are the distances from the source and field points to their respective points of tangency on the curved surface, and for (6.81) to be valid $\sqrt{kL/2}$ should be greater than m.

The total field in the illuminated part of the transition region is the incident field of geometrical optics plus $E^{\mathrm{d}}(P)$ given by (6.57), (6.58), and (6.81). $D(x)$ is the dominant term in (6.81); it is associated with the Fresnel (or Kirchhoff) diffraction by a half plane. As such it is independent of the polarization of the incident wave and the surface curvature. $G(\xi)$ can be regarded as a correction term containing this information; it has separate values for the s and h boundary conditions. The discontinuity in $D(x)$ at the shadow boundary $(x, \delta=0)$ exactly compensates the discontinuity in the incident field there so that the total high-frequency field is continuous at $\delta=0$. $G(\xi)$ is defined and presented graphically in [6.29]. Also $G(\xi)=\exp(-j\pi/4)\,[\tilde{p}(\xi)+1/(2\xi\sqrt{\pi})]$ and $\exp(-j\pi/4)\,[\tilde{q}(\xi)+1/(2\xi\sqrt{\pi})]$ for the s and h boundary conditions, respectively; the reflection coefficient functions $\tilde{p}$ and $\tilde{q}$ are described in [6.28] and (Ref. [6.9], Section 1.3.3).

This representation has been found to have good accuracy on the shadow boundary, and it can be shown that it blends with the GTD solution (6.57) for the deep shadow region. This blending it so first order; it is smoother for the h than the s boundary condition, and the larger kL the closer it occurs to the shadow boundary. Also this representation has been found to be quite accurate in the illuminated region near the shadow boundary, but it does not always join smoothly with the geometrical-optics field. Recently the author has become aware of the work of IVANOV [6.71] which appears to overcome this difficulty.

6.4.4. Two-Dimensional Problems

The preceding development can be applied to problems with a two-dimensional geometry by replacing

$$\sqrt{\frac{\varrho}{s(\varrho+s)}} \quad \text{with} \quad \frac{1}{\sqrt{s}},$$

$$\sqrt{\frac{d\eta_1}{d\eta_2}} \quad \text{or} \quad \sqrt{\frac{1}{\varrho}\,\frac{d\psi_1}{d\psi_2}} \quad \text{with} \quad 1,$$

dp_m with dM, a line of infinitesimal magnetic current, and $-jk/4\pi$ in (6.62) and (6.65b) with $-k\exp(j\pi/4)/\sqrt{8\pi k}$.

6.5. Applications

In applying the GTD one begins with ray tracing. The rays emanating from the primary source are considered first. The boundary surface of the radiating structure blocks the passage of the incident rays so that the space surrounding it is divided into an illuminated region occupied by the rays from the source and a shadow region where these rays do not penetrate. Upon encountering a perfectly-conducting surface the incident ray initiates a reflected ray from an interior point of the surface of a diffracted ray from edges, tips, or points of grazing incidence. The directions of these rays are determined by the laws of reflection and diffraction, which are corollaries to the generalized Fermat's principle; these laws have been described in the earlier sections. It should be noted that the reflected and diffracted rays also have illuminated regions which they cover and shadow regions which they do not penetrate. Moreover, these rays may encounter the boundary and give rise to higher-order diffracted or reflected rays. The field of the higher-order rays usually diminishes so rapidly with the number of successive diffractions that multiply-diffracted rays beyond the second or third order can be neglected. However in most two-dimensional problems (and some three-dimensional problems), it may be possible to sum the contributions from all the multiply-diffracted rays directly or to treat them by a self-consistent field procedure so that a closed form result is obtained.

Many problems are sufficiently simple so that the ray paths passing through a given field point can be determined without difficulty; in such cases the point of diffraction remains fixed as the field point varies or it moves about in a manner that can be described analytically. The paths of rays reflected from a plane surface are readily found by the method of images. However in the diffraction or reflection from a complex structure it may be necessary to employ a computer search routine to determine the points on the surface from which the rays emanate. These search procedures, such as the bisection method, employ the laws of diffraction or reflection.

It is evident that the GTD solution simplifies the surface radiation problem to the radiation from a finite array of scattering centers, which greatly reduces the time and cost of calculations. Since the GTD is a high-frequency method, these scattering centers cannot be spaced too closely. Generally speaking, they should be separated by a wavelength or more; however, the GTD solution often remains valid even for closer spacings. It is found that GTD solutions tend to fail gracefully as the frequency diminishes, until the low frequency or Rayleigh region is reached.

6.5.1. Reflector Antenna

The first example chosen to illustrate the application of the GTD is the calculation of the far-field pattern of an axially-symmetric parabolic reflector antenna. The essential components of our example are the reflector with a circular aperture of radius a and the feed positioned at its focus F, as shown in Fig. 6.10.

The geometrical optics far-field

$$E^{go}=\begin{cases}E^{f}, & \pi-\alpha>\theta>\delta\\ 0\ , & \pi-\alpha<\theta\leqq\pi\ ,\end{cases}\tag{6.82}$$

where E^{f} is the field of the feed, which is either calculated or measured and θ is the polar angle measured from the z-axis. A small angular sector $\delta\approx 5(ka)^{-1}$ in the forward axial direction has been excluded from the GTD solution, because of the difficulties encountered when there is a confluence of a reflection boundary and a caustic of the diffracted rays. The field in this region can be determined by the current-distribution method or the aperture-field method (Ref. [6.14], Chapters 6 and 9) and [6.32].

Let us calculate the pattern at the point P in the plane ϕ, $\pi+\phi$. This plane intersects the edge of the reflector at 1 and 2. Diffracted rays are induced at each point on the edge of the reflector, but only the straight line paths joining F and P which pass through the Points 1 and 2 satisfy (6.28). The paths F1P and F2P are the minimum and maximum distances between F and P which include a point on the edge of the reflector.

The ray singly-diffracted from edge 2 crosses the aperture and induces a doubly-diffracted ray at edge 1. The contribution to the far field from

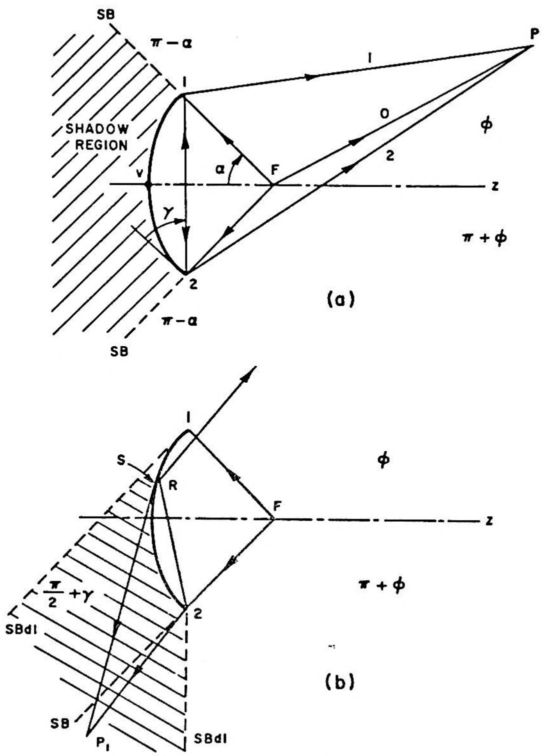

Fig. 6.10a and b. Reflector antenna showing diffracted and reflected rays

the rays singly- and doubly-diffracted from the edge at 1 can be written as

$$E^{\mathrm{d}}(1) = \Big[E^{\mathrm{f}}(s', \pi-\alpha, \phi)\cdot \underset{\sim}{D}(\psi_2, \psi_1; \pi/2) + E^{\mathrm{f}}(s', \pi-\alpha, \phi+\pi)\cdot \underset{\sim}{D}(\gamma, \psi_1; \pi/2)\cdot \underset{\sim}{D}(\psi_2, \gamma; \pi/2) \cdot j\,\frac{\mathrm{e}^{-j2ka}}{\sqrt{2a}}\Big]\sqrt{\frac{a}{\sin\theta}}\;\frac{\mathrm{e}^{-j(kR-ka\sin\theta)}}{R} \tag{6.83}$$

in which

$$\psi_1 = \gamma + \frac{\pi}{2} - \alpha\,,$$

$$\psi_2 = \gamma + \frac{\pi}{2} + \theta\,,$$

s' is the distance from F to the edge of the reflector, and R is the distance from P to the center of the aperture, which is chosen as the phase reference.

The factor j appears in the second term because there is a caustic on the ray which crosses the aperture. The ray diffracted from 1 is shadowed in the region $\pi/2 < \theta < \pi/2 + \gamma$, $\phi + \pi$ shown in Fig. 6.10b. The discontinuity in the geometrical-optics field at the shadow boundary $(\pi - \alpha, \phi)$ is compensated by the discontinuity in the field of the ray singly-diffracted from 1, and the discontinuity in the field of the ray singly-diffracted from 2 is compensated by the field of the ray doubly-diffracted from 1. The field $E^{d}(2)$ of the rays singly- and doubly-diffracted from 2 has a similar form. The fields of the higher-order multiply-diffracted rays could be included in the solution, but this contribution is insignificant when the aperture diameter is greater than a few wavelengths.

The field of the ray diffracted from the edge at 2 and then reflected from R on the concave side of the reflector is given by

$$E^{dr}(2, R) = -E^{f}(s', \pi - \alpha, \phi + \pi) \cdot \underset{\sim}{D}(\psi_r, \psi_1; \pi/2) \cdot \underset{\sim}{R} \sqrt{\frac{|\varrho|}{s(\varrho + s)}} \sqrt{|\varrho_1 \varrho_2|}\, e^{-jks} \frac{e^{-j(kR + \phi_R)}}{R}, \qquad \theta_2 < \theta < \theta_1 \tag{6.84}$$

in which ψ_r is the angle between the ray diffracted to R and the plane tangent to the reflector at 2, s is the distance between 2 and R, ϱ is the caustic distance of the edge diffracted ray (it is negative), ϱ_1, ϱ_2 are the principal radii of curvature of the reflected wavefront at R, f is the focal distance of the reflector, ϕ_R is the phase factor relating this contribution to the phase center, $\theta_1 = 2\tan^{-1}(2f/a) - \pi/2$, and $\theta_2 = \tan^{-1}(4f/a)$.

A caustic occurs between 2 and R and a second caustic between R and P, which accounts for the minus sign preceding E^{f}. $E^{dr}(2, \mathrm{R})$ vanishes outside the interval $\theta_2 < \theta < \theta_1$. θ may be expressed in terms of ψ_r but in calculating the pattern, we wish to determine ψ_r (and the Point R) as a function of θ. This can be done by a simple computer search routine such as the bisection method mentioned earlier. Equations (6.83) and

(6.84) simplify markedly in the H- and E-plane, where E^{f} is usually parallel or perpendicular to the edge at 1 and 2. For example, in the H-plane $E^{\mathrm{f}} \cdot \underset{\sim}{D} = -E^{\mathrm{f}} \cdot \underset{\sim}{D} \cdot \underset{\sim}{R} = E^{\mathrm{f}} D_{\mathrm{s}}$ and in the E-plane $E^{\mathrm{f}} \cdot \underset{\sim}{D} = E^{\mathrm{f}} \cdot \underset{\sim}{D} \cdot \underset{\sim}{R} = -E^{\mathrm{f}} D_{\mathrm{h}}$. There is a similar ray diffracted from edge 1 and reflected from the concave surface.

In the region $\pi - \delta > \theta > \delta$

$$E(P) = E^{\mathrm{go}} + E^{\mathrm{d}}(1) + E^{\mathrm{d}}(2) + E^{\mathrm{dr}}(1, \mathrm{R}) + E^{\mathrm{dr}}(2, \mathrm{R}) . \tag{6.85}$$

A more complete analysis would include the surface rays exctited at 1 and 2; however the contribution from these rays is generally very weak.

The rear axis of the reflector is a caustic of the diffracted rays, so the GTD can not be used here without modification. In the caustic region $\pi - \delta < \theta \leqq \pi$, the field can be calculated from an integral representation using the equivalent electric

$$I(\phi) = \frac{-\hat{e} \cdot E^{\mathrm{f}}}{Z_{\mathrm{c}}} D_{\mathrm{s}}(2\pi - \gamma, \psi_1 ; \pi/2) \sqrt{\frac{8\pi}{k}}\, \mathrm{e}^{-j\frac{\pi}{4}} \tag{6.86}$$

and magnetic

$$M(\phi) = -(\hat{e} \times \hat{s}') \cdot E^{\mathrm{f}} D_{\mathrm{h}}(2\pi - \gamma, \psi_1 ; \pi/2) \sqrt{\frac{8\pi}{k}}\, \mathrm{e}^{-j\frac{\pi}{4}} \tag{6.87}$$

ring currents flowing on the dege of the reflector [6.32–6.34]. This procedure is accurate for $\theta = \pi$, and it is a good approximation in the caustic region joining smoothly with the field of the two edge diffracted rays, if the diffraction coefficient is slowly varying in this region.

AFIFI [6.35] has measured the H-plane pattern of a parabolic reflector antenna mounted on a ground plane and fed by a monopole. This is a desirable configuration to test our solution, because the scattering from the feed support has been neglected. The measured pattern and the pattern calculated from our GTD solution are shown in Fig. 6.11. The two patterns are seen to be in good agreement. In the range of aspects $10^\circ < \theta < 70^\circ$ the pattern is quite frequency sensitive. If the frequency used to calculate the pattern is changed by only 5 percent, the agreement between the calculated and measured patterns is greatly improved.

The wide angle side lobes also can be calculated by physical optics, but the computational time is much greater and the results are less accurate. The GTD can be applied to calculate the patterns of a wide class of reflector antennas including those with subreflectors, where the scattering from the subreflector must be taken into account.

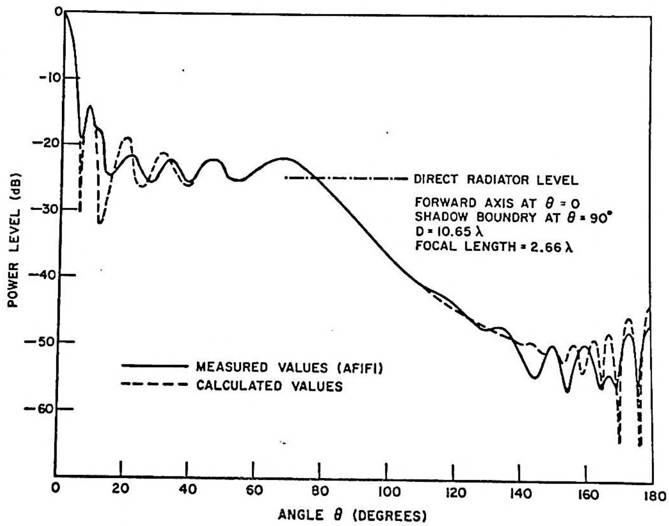

Fig. 6.11. H-plane pattern of a parabolic reflector antenna with a dipole feed

6.5.2. Slot in an Elliptic Cylinder

As a second example of the application of the GTD we will briefly consider the radiation from an axial slot in a perfectly-conducting elliptic cylinder. The far-zone pattern is to be calculated in a plane perpendicular to the axis of the slot so that the surface rays involved are torsionless. The rays which contribute to the field in the illuminated and shadow regions are depicted in Fig. 6.12. The equation

$$y_d = \pm a \Big/ \sqrt{1 + \left(\frac{b}{a}\right)^2 \tan^2 \phi} \tag{6.88}$$

locates the points of diffraction Q_2 and Q_2' as a function of the aspect angle ϕ, which together with b and a is defined in Fig. 6.12. Equations (6.61), (6.62), and (6.78) and the expressions for the GTD parameters and $g(\xi)$ are used to calculate the diffracted field. The finite width of the slot (0.34 wavelength) is taken into account by an array of 5 magnetic dipoles in the aperture. In Fig. 6.13 calculated patterns are compared with

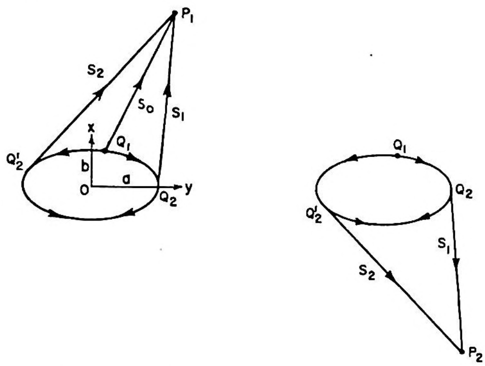

Fig. 6.12. Rays emanating from a source on a curved surface

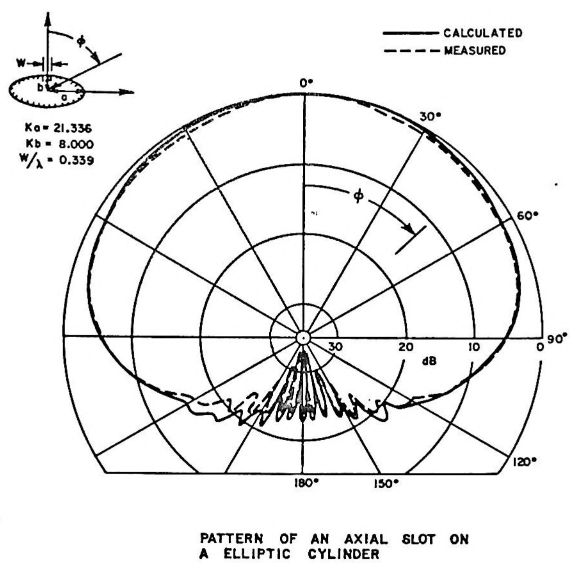

Fig. 6.13. Pattern of an axial slot on an elliptic cyclinder

measured patterns [6.27], and the agreement between the two patterns is seen to be good. The discrepancy between the calculated and measured patterns is no worse than that between the two halves of the measured pattern about its vertical axis.

As noted earlier, the formulas given in this chapter can be applied formally to cases where there are torsional surface rays, such as a pattern calculation in an oblique plane in the present example. Since the dominant term in (6.61) containing F_s is independent of torsion to first order, the torsional effects are not too noticeable except at the lower levels of the patterns. On the other hand, in calculating the mutual coupling between slots, which is exclusively a shadow region phenomenon, the torsional effects are much more evident than in the corresponding radiation pattern.

In the two examples considered thus far the GTD has been used to calculate far fields, but there is no reason why it cannot be used to calculate near fields provided that the field point is not too close to a point of diffraction, which is roughly a wavelength in the case of edge diffraction.

6.5.3. Monopole Antenna Near an Edge

Consider a monopole radiating in the presence of an edge, as shown in Fig. 6.14. This example is chosen to demonstrate the flexibility of the GTD by combining it with the moment method described in the earlier chapters. For simplicity pulse basis functions and impulse test functions are employed. Dividing the monopole into N segments of length Δ, the moment method solution is given compactly by

$$-E^{\mathrm{i}}_m = \sum_{n=1}^{N} Z_{mn} I_n, \qquad m = 1, 2, \ldots, N, \tag{6.89}$$

where E^{i}_m is the axial component of the incident electric field at the center of the mth segment, I_n is the constant current on the nth segment, and Z_{mn} is an element of the generalized impedance matrix, which describes the total interaction between the m and nth segments.

Let the current on the nth segment be the source of the electric field E_m at the center of the mth segment. The impedance element $Z_{mn} = E_{zm}/I_n$ in which E_{zm} is the axial (or z) component of E_m.

$$E_{zm} = E^{\mathrm{o}}_{zm} + E^{\mathrm{r}}_{zm} + E^{\mathrm{d}}_{zm}, \tag{6.90}$$

where E^{o}_{zm} is due to the free-space radiation from I_n and E^{r}_{zm} is due to reflection from the horizontal surface of the wedge, which may be found from the image of I_n as indicated in Fig. 6.14. It follows then that for

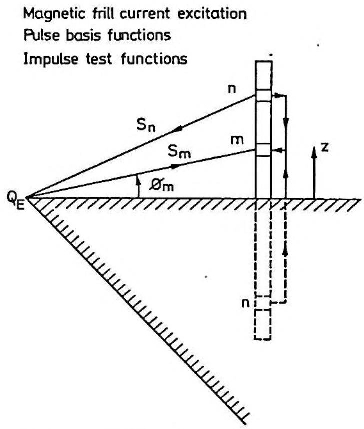

Fig. 6.14. Monopole on a wedge

$\Delta \ll \lambda$ and $|z_n - z_m|$,

$$Z^{o}_{mn} + Z^{r}_{mn} \approx \frac{jkZ_c\Delta}{4\pi}\left[1 - \frac{1}{k^2}\frac{\partial^2}{\partial z\,\partial z'}\right]\frac{e^{-jkr}}{r}\Bigg|_{\substack{z=z_m\\ z'=\pm z_n}} \tag{6.91}$$

with $r = \sqrt{(z-z')^2 + a^2}$ in which a is the radius of the monopole; $z' = \pm z_n$ implies that (6.91) has two terms.

The axial component of the diffracted electric field E^{d}_{sm} is determined by the GTD. The pertinent ray path is $n\mathrm{Q_E}m$, and

$$Z^{d}_{mn} = \frac{jkZ_c\Delta}{4\pi}\,\frac{D_h\left(\phi_m, \phi_n; \dfrac{\pi}{2}\right)}{\sqrt{S_n S_m (S_n + S_m)}}\,e^{-jk(S_n+S_m)}\cos\phi_m \cos\phi_n. \tag{6.92}$$

The current at N points on the monopole is given by the current column matrix

$$[I] = [Z]^{-1}[E^{i}]$$

in which $[Z]^{-1}$ is the inverse of the generalized impedance matrix and $[E^{i}]$ is the column matrix with N elements E^{i}_{m}. The GTD-moment

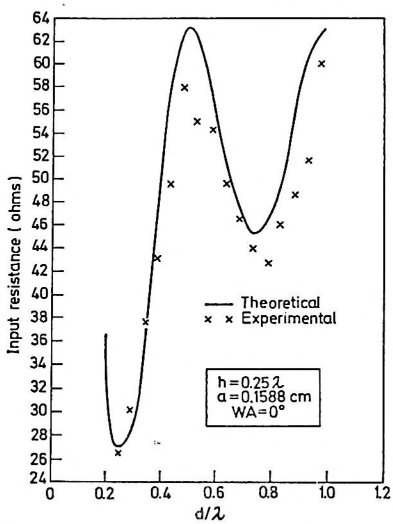

Fig. 6.15. Input resistance of a monopole at the center of an octagonal plate

method solution described here is based on the work of THIELE and NEWHOUSE [6.36], who applied it to calculate the input impedance to a monopole at the center of square, octagonal and circular plates. The coaxial feed is modelled by a magnetic frill current (Ref. [6.37], Appendix I), which is the source of E_m^i, and in these examples the wedge angle $\mathrm{WA}=(2-n)\pi=0$. In Fig. 6.15 calculated values of the input resistance for the octagonal plate case are compared with measured values. The agreement is reasonably good considering the difficulties encountered with the measurements. The measured and calculated values of the input reactance compare similarly. The length of the monopole is h, its radius is a, and the perpendicular distance from its base to the sides of the octagonal plate is d.

It is clear that this hybrid GTD-moment method can be applied to a general wire antenna configuration. Moreover it can be readily extended to a receiving wire antenna. In this case, referring to the geometry in Fig. 6.14, E_m^i consists of directly-radiated, reflected and edge-diffracted terms.

6.5.4. Discussion

The examples presented in the preceding subsections are only a small sample of the problems that have been treated by the GTD. In the early history of the theory KELLER and his co-workers applied the GTD to determine the scalar diffraction by slits, circular apertures, cylinders, cylinder tipped-half planes, cones, spheres, and spheroids; in addition they treated the electromagnetic diffraction by spheres, cones, and arbitrary cylinders illuminated at oblique incidence. In their papers the pertinent ray analysis is given along with expressions for the diffracted fields away from the radiating body; however the solutions are not valid in the transition regions adjacent to shadow and reflection boundaries. A convenient review of these papers is given in [6.12]; also many of their results are described in [6.9] along with some additional results for the diffraction by a strip. An improved GTD solution for the diffraction by a cylinder-tipped half plane using the diffraction coefficients and attenuation constants in Table 6.2 is described in [6.38]. Additional contributions to the electromagnetic backscatter from cones are presented in [6.33, 6.39–6.43], but the GTD analysis is still not complete. For example, work remains to be done on the base-tip interaction, particularly with regard to the transition phenomena associated with the shadowing of the base by the tip. The electromagnetic backscatter by circular discs is treated in [6.44, 6.45]. The solution reported in the latter reference contains a type of doubly-diffracted ray omitted in the former; however the treatment of the fields of the doubly-diffracted rays on the illuminated and shadow side of the disc and the factor of 1/2 required at grazing incidence is obscure. The backscatter from rectangular plates is described in [6.46], where the problem is reduced to that of a strip for the GTD analysis. In [6.47] a GTD solution is presented for the scattering by a rectangular cylinder which is illuminated by the field of a line source. Since the edge diffraction coefficients in (6.33) are used, the solution is valid in the transition regions. Calculated patterns are found to be in excellent agreement with those calculated by the moment method. A comparison of GTD and moment method solutions for the strip and the two-dimensional corner and trough is carried out in [6.48]; the patterns calculated from the GTD solutions, which are valid in the transition regions, are in excellent agreement with those obtained by the moment method, for the intermediate-sized structures (0.5 to 5 λ). The GTD has also been applied to calculate the scattering from thin, curved wires [6.49]. The patterns are found to be in good agreement with those calculated by the variational method.

The GTD has been applied to a variety of antenna problems. The parabolic reflector antenna is treated in [6.32], and calculations of the scattering from a hyperboloidal subreflector are presented in Chapter 7; Subsection 7.3.4. Ray-optical methods are employed to determine the aperture reflection coefficients and radiation patterns of parallel-plate waveguides in [6.50–6.55]. The related problem of the E- and H-plane patterns of horn antennas was studied in [6.56–6.58]. The calculation of the patterns in the principal planes is facilitated by reducing the geometry to a two-dimensional configuration; however in the H-plane calculation, one may also get significant contributions from rays diffracted from the edges parallel to this plane. The reflection coefficient for the junction of a rectangular waveguide and an H-plane sectorial horn is calculated in [6.59]. The diffraction coefficient in (6.33) is needed to get accurate results for very small flare angles where overlapping transition regions occur at the junction. In [6.60] the GTD is used to investigate the gain and radiation pattern of a conical horn excited by a circular waveguide operating in the TE_{11} mode.

The examples discussed thus far have involved relatively simple shapes, but the GTD also can be used to calculate the radiation from complex structures. The radiation pattern of a linerar array of pistons mounted in one face of a rigid, rectangular box is considered in [6.61]. Although this is an acoustics problem, it has much in common with an array of slots in a rectangular ground plane. When the contributions from the incident (geometrical optics) ray plus all the rays singly- and doubly-diffracted from the 12 edges of the box are taken into account, the resulting calculated patterns are in excellent agreement with measured patterns. The GTD has been employed to calculate the patterns of slots and monopoles positioned on the fuselage of an aircraft [6.26, 6.62]. Even though the aircraft is modelled in its most basic form, so that only the fuselage and wings are considered in the roll plane analysis, the ray analysis is not simple. In addition to the incident ray, a surface ray is launched on the fuselage, and the surface ray sheds a diffracted ray, which in turn may be reflected and diffracted from the wings. Generally speaking, the agreement between calculated and measured patterns is excellent. The GTD has been used to predict the patterns of satellite antennas [6.63, 6.64]. The configurations studied consist of dipoles radiating in the presence of finite circular and rectangular cylinders and monopoles mounted on the cylinder. Calculated patterns, largely based on preliminary results, appear to be in quite good agreement with measured patterns. The edge diffraction coefficients described in this chapter are employed in [6.26, 6.61–6.64].

For simplicity the discussion in this chapter has been restricted to the radiation from hard, soft and perfectly-conducting surfaces in isotropic, homogeneous media, but the GTD can be extended to treat bodies in inhomogeneous media [6.65, 6.66] and anisotropic media

[6.67] and to bodies with penetrable [6.68] and impedance surfaces (Ref. [6.9], pp. 48–49, and [6.28]). A thorough treatment of ray-optical fields in inhomogeneous and anisotropic media is given in [6.3, 6.69].

6.6. Conclusions

In the geometrical theory of diffraction, the diffracted fields propagate in the same manner as the geometrical-optics field. The spreading of rays in a plane containing the edge caustic or the caustic or surface diffraction is determined from differential geometry; thus the field of a diffracted ray is determined in part by geometrical considerations and in part by wave considerations provided by the diffraction coefficients. Furthermore, it is assumed that the diffraction mechanism is, in effect, localized at an edge or shadow boundary, and that it functions independently of the other parts of the structure. The ultimate accuracy of the geometrical theory of diffraction appears to be limited by these two assumptions, particularly in the case of the smaller radiating structures.

Numerous comparisons of GTD solutions with asymptotic expansions, calculations based on convergent (exact) methods, and measurements have shown that the GTD provides a systematic approach to the high-frequency solution of a wide variety of antenna, scattering and propagation problems. In many instances the GTD solution is not only accurate at high frequencies, but also at relatively low frequencies, where the ratio of the characteristic dimension to wavelength is of order unity. However, presuming that the GTD is an asymptotic method, one expects it to fail as the frequency is reduced, regardless of the number of terms retained in the approximation. At sufficiently low frequencies the local behavior of reflection and diffraction break down.

As a purely ray-optical technique the GTD fails near caustics and in transition regions adjacent to shadow and reflection boundaries; however in this chapter we have shown that the GTD can be extended to calculate fields in the transition regions. As noted earlier, supplementary methods exist for treating the field at a caustic; often one can introduce an integral representation of the field where geometrical optics or the GTD is used to determine the equivalent source. If desired, the accuracy of the geometrical optics current can be improved by using Ufimstev's method [6.70].

The reason for using the GTD method stems from the significant advantages to be gained; namely

a) it is simple to use, and yields accurate results;

b) it provides some physical insight into the radiation and scattering mechanisms involved;

c) it can be used to treat problems for which exact analytical solutions are not available;

d) it can be combined readily with other methods such as the moment method.

References

6.1. R. K. LUNEBERG: *Mathematical Theory of Optics* (Brown University Notes Providence, 1944). Also published by (University of California Press, Berkeley, 1964).
6.2. M. KLINE: In *The Theory of Electromagnetic Waves* (Interscience Publishers Inc., New York, 1951), pp. 225–262. See also his chapter in *Electromagnetic Waves*, ed. by R. E. LANGER (University of Wisconsin Press, Madison, 1962), pp. 3–32.
6.3. M. KLINE, I. KAY: *Electromagnetic Theory and Geometrical Optics* (Interscience Publishers, New York, 1965).
6.4. J. B. KELLER, R. M. LEWIS, B. D. SECKLER: Comm. Pure Appl. Math. **9**, 208 (1973).
6.5. R. G. KOUYOUMJIAN: Proc. IEEE **53**, 864 (1965).
6.6. I. KAY, J. B. KELLER: J. Appl. Phys. **25**, 876 (1954).
6.7. D. LUDWIG: Comm. Pure Appl. Math. **19**, 215 (1966).
6.8. R. G. KOUYOUMJIAN, P. H. PATHAK: Proc. IEEE **62**, 1448 (1974).
6.9. J. J. BOWMAN, T. B. A. SENIOR, P. L. E. USLENGHI: *Electromagnetic and Acoustic Scattering by Simple Shapes* (North-Holland Publishing Co., Amsterdam, 1969).
6.10. J. B. KELLER: In "Proc. Symposium on Microwave Optics", p. II, McGill University (1953) Astia Document AD 211500 (1959), pp. 207–210.
6.11. J. B. KELLER: In *Calculus of Variations and its Applications*, ed. by L. M. GRAVES (McGraw-Hill Book Co., New York, 1958), pp. 27–52.
6.12. J. B. KELLER: J. Opt. Soc. Am. **52**, 116 (1962).
6.13. M. BORN, E. WOLF: *Principles of Optics*, 4th ed. (Pergamon Press, Oxford, 1970), pp. 753, 754.
6.14. S. SILVER: *Microwave Antenna Theory and Design* (McGraw Hill Book Co., New York, 1949), pp. 119–122.
6.15. P. H. PATHAK, R. G. KOUYOUMJIAN: "The Dyadic Diffraction Coefficient for a Perfectly-Conducting Wedge", Report 2183-4, Electro-Science Laboratory, The Ohio State University, Columbus, Ohio 1973).
6.16. S. N. KARP, J. B. KELLER: Optica Acta **8**, 61 (1961).
6.17. L. KAMINETZKY, J. B. KELLER: SIAM J. Appl. Math. **22**, 109 (1972).
6.18. T. B. A. SENIOR: IEEE Trans. Antennas Propagation AP-**20**, 326 (1972).
6.19. K. M. SIEGEL, J. W. CRIPSIN, E. SCHENSTED: J. Appl. Phys. **26**, 309 (1955).
6.20. L. B. FELSEN: IRE Trans. Antennas Propagation AP-**5**, 121 (1957).
6.21. B. R. LEVY, J. B. KELLER: Comm. Pure Appl. Math. **12**, 159 (1959).
6.22. J. B. KELLER, B. R. LEVY: IRE Trans. Antennas Propagation AP-7, S 52.
6.23. W. FRANZ, K. KLANTE: IRE Trans. Antennas Propagation AP-7, S 68 (1959).
6.24. S. HONG: J. Math. Phys. **8**, 1223 (1967).
6.25. D. R. VOLTMER: "Diffraction by Doubly Curved Convex Surfaces", Ph.D. Dissertation, The Ohio State Univ., Columbus, Ohio (1970).
6.26. W. D. BURNSIDE: "Analysis of On-Aircraft Antenna Patterns", Report 3390-1, Electro-Science Laboratory, The Ohio State Univ., Columbus, Ohio (1972).
6.27. P. H. PATHAK, R. G. KOUYOUMJIAN: Proc. IEEE **62**, 1438 (1974).
6.28. N. A. LOGAN: "General Research in Diffraction Theory", Vols. I, II, Reports LMSD-288087, 288088, Lockheed Aircraft Corporation, Missiles and Space Division, Sunnyvale, Calif. (1959). See also N. A. LOGAN, K. S. YEE: In *Electro-*

magnetic Waves, ed. by R.E.LANGER (University of Wisconsin Press, Madison, 1962), pp. 139–180.
6.29. J.R.WAIT, A.M.CONDA: J. Res. of N.B.S. **63D**, 181 (1959).
6.30. V.A.FOCK: *Electromagnetic Diffraction and Propagation Problems* (Pergamon Press, Oxford, 1965), pp. 134–146.
6.31. A.S.GORIAINOV: Radio Eng. Electron. (USSR) **3**, 23 (1958) English translation of Radiotechn. i Elektron. 3, 603 (1958).
6.32. P.A.J.RATNASIRI, R.G.KOUYOUMJIAN, P.H.PATHAK: "The Wide Angle Side Lobes of Reflector Antennas", Report 2183-1, Electro-Science Laboratory, The Ohio State Univ., Columbus, Ohio (1970).
6.33. C.E.RYAN, JR., L.PETERS, JR.: IEEE Trans. Antennas Propagation **AP-17**, 292 (1969).
6.34. C.E.RYAN, JR., L.PETERS, JR.: IEEE Trans. Antennas Propagation **AP-18**, 275 (1970).
6.35. M.S.AFIFI: In *Electromagnetic Wave Theory*, Part 2, ed by J.BROWN (Pergamon Press, Oxford, 1967), pp. 669–687.
6.36. G.A.THIELE, T.H.NEWHOUSE: IEEE Trans. Antennas Propagation **AP-23**, 62 (1975).
6.37. G.A.THIELE: In *Computer Techniques in Electromagnetics*, ed. by R.MITTRA (Pergamon Press, Oxford, 1973), pp. 7–95.
6.38. R.G.KOUYOUMJIAN, W.D.BURNSIDE: IEEE Trans. Antennas Propagation **AP-18**, 424 (1970).
6.39. M.E.BECHTEL: Proc. IEEE **53**, 877 (1965).
6.40. R.A.ROSS: IEEE Trans. Antennas Propagation **AP-17**, 241 (1969).
6.41. T.B.A.SENIOR, P.L.E.USLENGHI: Radio Science **6**, 393 (1971).
6.42. W.D.BURNSIDE, L.PETERS, JR.: Radio Science **7**, 943 (1972).
6.43. T.B.A.SENIOR, P.L.E.USLENGHI: Radio Science **8**, 247 (1973).
6.44. R.V.DEVORE, R.G.KOUYOUMJIAN: "The Back Scattering from a Circular Disk", URSI-IRE Spring Meeting, Washington, D.C. (1961).
6.45. E.F.KNOTT, T.B.A.SENIOR, P.L.E.USLENGHI: Proc. IEE (London) **118**, 1736 (1971).
6.46. R.A.ROSS: IEEE Trans. Antennas Propagation **AP-14**, 329 (1966).
6.47. R.G.KOUYOUMJIAN, N.WANG: "Diffraction by a Perfectly Conducting Rectangular Cylinder which is Illuminated by an Array of Line Sources", Report 3001-7, Electro-Science Laboratory, The Ohio State Univ., Columbus, Ohio (1973).
6.48. L.L.TSAI, D.R.WILTON, M.G.HARRISON, E.H.WRIGHT: IEEE Trans. Antennas Propagation **AP-20**, 705 (1972).
6.49. J.B.KELLER, D.S.AHLUWALIA: SIAM J. Appl. Math. **20**, 390 (1971).
6.50. R.B.DYBDAL, R.C.RUDDUCK, L.L.TSAI: IEEE Trans. Antennas Propagation **AP-14**, 574 (1966).
6.51. R.C.RUDDUCK, L.L.TSAI: IEEE Trans Antennas Propagation **AP-16**, 84 (1968).
6.52. C.E.RYAN, JR., R.C.RUDDUCK: IEEE Trans. Antennas Propagation **AP-16**, 490 (1968).
6.53. R.C.RUDDUCK, D.C.F.WU: IEEE Trans. Antennas Propagation **AP-17**, 797 (1969).
6.54. H.Y.YEE, L.B.FELSEN, J.B.KELLER: SIAM J. Appl. Math. **16**, 268 (1968).
6.55. L.B.FELSEN, H.Y.YEE: IEEE Trans. Antennas Propagation **AP-16**, 268 and 360 (1968).
6.56. J.S.YU, R.C.RUDDUCK, L.PETERS, JR.: IEEE Trans. Antennas Propagation **AP-14**, 138 (1966).
6.57. J.S.YU, R.C.RUDDUCK: IEEE Trans. Antennas Propagation **AP-17**, 651 (1969).
6.58. C.A.MENTZER, L.PETERS, JR., R.C.RUDDUCK: Submitted for publication.

6.59. T. Hua: "The Reflection Coefficient of a Horn-Waveguide Junction", M.Sc. Thesis, The Ohio State Univ., Columbus, Ohio (1970).
6.60. M. A. K. Hamid: IEEE Trans. Antennas Propagation AP-**16**, 520 (1968).
6.61. D. L. Hutchins, R. G. Kouyoumjian: J. Acoust. Soc. Am. **45**, 485 (1969).
6.62. W. D. Burnside, R. J. Marhefka, C. L. Yu: "Roll Plane Analysis of On-Aircraft Antennas" Pre-print 139 (AGARD Conference on Antennas for Avionics, Munich, Germany, 1973).
6.63. F. Molinet, L. Saltiel: "High Frequency Radiation Pattern Prediction for Satellite Antennas", Final Report ESTEC Contract 1820/72 HP, Laboratoire Central de Telecommunications, Velizy-Villacoublay, France (1973).
6.64. J. Bach, K. Pontoppidan, L. Solymar: "High Frequency Radiation Pattern Prediction for Satellite Antennas", Final Report ESTEC Contract 1821/72 HP, The Technical University of Denmark, Lyngby (1973).
6.65. B. D. Seckler, J. B. Keller: J. Acoust. Soc. Am. **31**, 192 (1959).
6.66. R. M. Lewis, N. Bleistein, D. Ludwig: Comm. Pure Appl. Math. **20**, 295 (1967).
6.67. B. Rulf, L. B. Felsen: In *Quasi-Optics*, ed. by J. Fox (Polytechnic Press, Brooklyn, 1964), pp. 107–149.
6.68. H. M. Nussenzveig: In *Methods and Problems of Theoretical Physics*, ed. by J. E. Bowcock (North Holland Publishing Co., Amsterdam, 1970).
6.69. L. B. Felsen, N. Marcuvitz: *Radiation and Scattering of Waves* (Prentice-Hall, Inc., Englewood Cliffs, N.J., 1973).
6.70. P. Ya. Ufimtsev: *Metod Krayevykh Voiln v Fizicheskoy Teorii Difraktsii* (Sovetskoye Radio, 1962). For an English translation see Foreign Technology Division, Document ID No. FTD-HC-23-259-71 (1971).
6.71. V. I. Ivanov: USSR Comput. Math. and Math. Phys. **2**, 216 (1971).

Subject Index